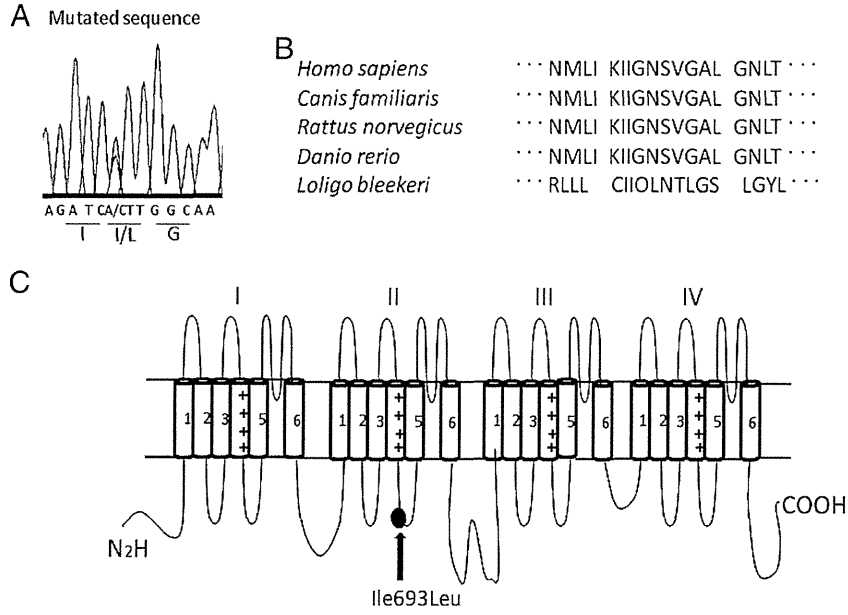

Fig. 2. A: DNA sequencing of the mutant region shows the transition of A to C at the nucleotide in position 2077 resulting in the substitution isoleucine (I) to leucine (L) at aminoacid in position 693 (I693L).B: Isoleucine residue in position 693 in Nav1.4 channel is preserved among homologs in many species.C: Schematic of the α subunit of Nav1.4 channel showing the six transmembrane segments (1–6) of each of the four domains (I–IV) and the location of p.I693L mutation (gray point).

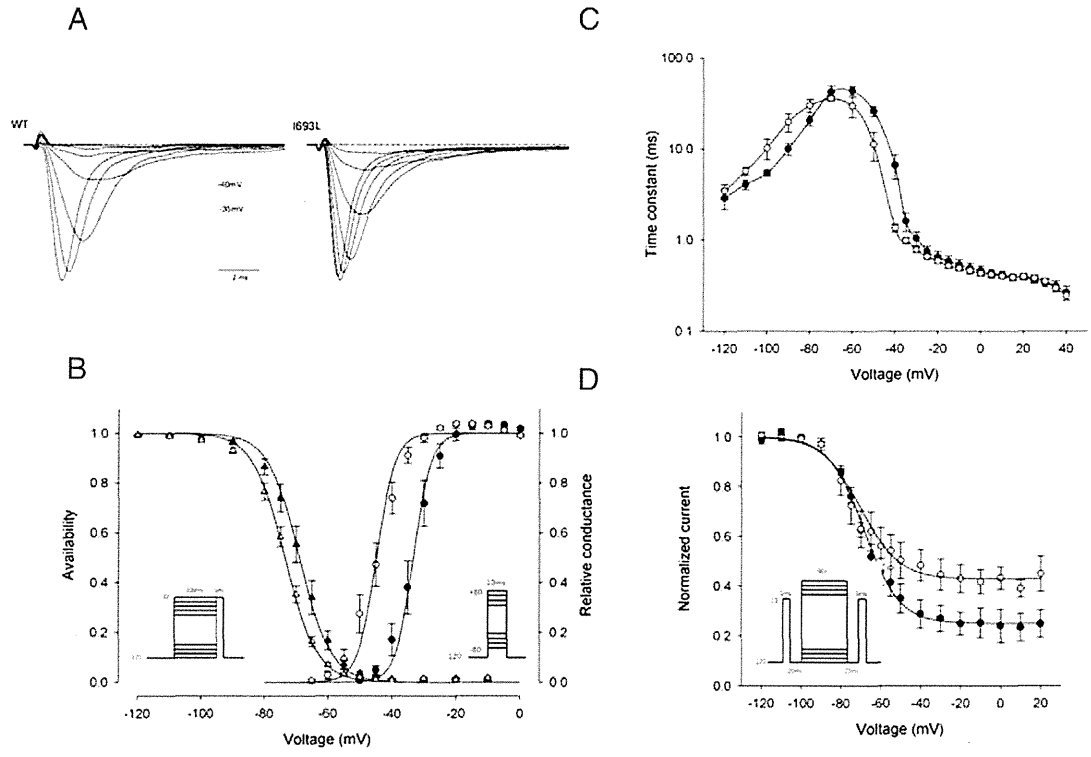

Fig. 3. A: Representative normalized currents recorded from HEK cells transfected with wild-type (WT) and I693L mutant channel and elicited by a series of 10 ms step pulse depolarizations from a holding potential of −120 mV to +40 mV in 5 mV increments. Activation is enhanced in I693L mutant channels.B: Activation (right-hand curves) for the wild-type ○ and I693L ● channels measured as the relative conductance of the peak sodium current elicited by depolarizing pulse from a holding potential of −120 mV to +40 mV (protocol in right inset). The activation voltage dependence of I693L mutant was shifted in the direction of hyperpolarization ($p<0.001$). Steady state fast inactivation (left-hand curves) for the wild-type △ and p.I693L ▲ channels measured as the relative peak current elicited by a −10 mV pulse after a 300 ms conditioning (protocol in left inset). We observed a shift towards negative voltages of the mutant constructs ($p=0.009$).C: Voltage dependence of the fast inactivation kinetics for the wild-type ○ and I693L ● channels measured by combining the data from three protocols (see results): a two-pulse recovery protocol (−120 mV to −80 mV), a two-pulse entry protocol (−70 mV to −40 mV) and a single-pulse relaxation protocol (−35 mV to +40 mV). The time constant for I693L channels was slightly slower at the negative voltages measured with the recovery protocol (n.s. $p>0.05$) and faster at the intermediate voltages measured with the entry protocol (from −50 mV to −35 mV $p<0.05$) than the wild-type. No difference was observed at more depolarized voltage.D: Peak sodium current elicited by a −10 mV test pulse was measured after a 60 s conditioning followed by a 20 ms gap at −120 mV to allow recovery from fast inactivation (protocol in the inset). The maximum extent of slow inactivation (1–I0) was smaller for I693L channels ●, revealing its impairment in comparison with the wild-type ○.

Please cite this article as: Yoshinaga H, et al, A novel mutation in SCN4A causes severe myotonia and school-age-onset paralytic episodes, J Neurol Sci (2012), doi:10.1016/j.jns.2011.12.015

Table 1
Gating parameter for WT and mutant Nav 1.4.

	Activation		Fast inactivation		Slow inactivation		
	V1/2(mV)	*k* (mV)	V1/2(mV)	*k* (mV)	V1/2(mV)	*k* (mV)	I0
WT	−33.3 ± 1.5 (9)	2.8 ± 0.4	−68.9 ± 1.6 (9)	5.0 ± 0.2	−68.3 ± 1.4 (5)	8.9 ± 1.1	0.25 ± 0.0522
p.I693L	−44.9 ± 1.5** (16)	2.9 ± 0.2	−73.5 ± 0.9* (5)	5.1 ± 0.2	−70.1 ± 3.3 (6)	9.6 ± 1.6	0.43 ± 0.0446*

Values are means + S.E.M, with number of experiments in parenthesis * significantly different from WT. P<0.05.
**significantly different from WT. P<0.001.

3. Discussion

Prior to identification of the sodium channel mutation, this patient was initially diagnosed as having a myogenic type of Schwartz–Jampel syndrome because of his characteristic appearance with severe myotonia [1,11]. The confusion between Schwartz–Jampel syndrome and sodium channelopathy was previously reported in a patient with myotonia permanence caused by G1306E mutation of SCN4A [4]. Our patient may also correspond to myotonia permanence, and he exhibited severe myotonic symptoms as apneic episodes from the neonatal period. Several patients with a *SCN4A* mutation, who showed severe symptoms including respiratory distress from an early neonatal period have also been reported [7,8]. One of these cases resembled Schwartz–Jampel syndrome [8].

Our patient showed severe myotonic episodes in his early infancy and then subsequent paralytic episodes. This case provides an example of the complexity and overlap of the clinical features of the sodium channel myotonic disorders, which sometimes make their classification difficult.

Some medications, including local anesthetics, anticonvulsants, and antiarrhythmics such as mexiletine, have shown efficacy for myotonic sodium channelopathies by blocking the sodium channel [2,15]. A carbonic anhydrase inhibitor, acetazolamide, is known to prevent paralytic attack but its antimyotonic action is in question. The myotonia of our patient showed a good response to mexiletine, phenytoin and acetazolamide, although carmabazepin showed little effect. Further studies are needed to understand the difference in efficacy between these drugs and the effects of acetazolamide.

The recently proposed standardized protocols involving short and long exercise tests in electromyographic analysis have improved the diagnosis of the subgroup of mutations in muscle channelopathies [12,13]. Fournier et al. [13] reported that combining the responses to several tests defined five electromyographic patterns that correspond to the subgroups of mutations. We applied their protocol to our patient and defined the response as pattern III [11] in which excitability is not impeded by any of the exercise trials. In their report [11], patients carrying G1306A or I693T (same locus on Nav 1.4 as ours [16]) sodium channel mutation also exhibited pattern III.

Functional analysis of the mutant channel revealed that the activation of the mutant channel was markedly enhanced in concordance with the enhanced excitability of our patient. However hyperpolarized shift of the steady-state inactivation curve which should reduce excitability, was also in a milder way observed in the mutant channel. The former may prevail over the latter, explaining the enhanced excitability which contributes to myotonia. Other mutations such as V445M [17], L689I [18], I704M, including the aforementioned I693T [16], have been found to similarly enhance both activation and fast inactivation and are often associated with myotonia.

Also, our data showed disrupted slow inactivation in the mutant construct, a defect which is expected to predispose to prolonged attack of paralysis. Our patient started to show episodic weakness recently. Again, I693T mutation showed an enhancement of activation with a slight shift towards hyperpolarized voltages for the steady state inactivation as well as a severely impaired slow inactivation [16]. The channel gating defects for I693T and its electromyographic pattern are strikingly similar with those observed for I693L. Unexpectedly, the I693T patient suffered from cold-induced weakness with a very mild myotonia [16]. The difference in hydrophobicity between the two mutated amino acids or the underlining genetic or environmental factors such as drug treatment can possibly modulate the expression of the disease.

Two other mutations, L689I and T70M, have been reported in the intracellular loop linking segments 4–5 of domain II in *SCN4A* [18]. Both have a phenotype of hyperkalemic periodic paralysis with a predominant weakness. The functional analysis of these mutant channels again revealed an enhancement of activation, and an impaired slow inactivation to a similar extent as for I693L mutant. These data and ours confirm the fact that the IIS4-S5 linker is one of the determinant regions for the sodium channel slow inactivation and to a various extent for the activation.

4. Conclusion

Further study of the genotype–phenotype correlations through individual cases will increase our knowledge of the variability of signs in this group of diseases and may also provide us with deeper insight into the function of the various regions of sodium channel proteins.

Acknowledgement

We thank Dr. Steve Cannon, University of Texas, for providing the expression vectors. This study was supported by Grants-in-Aids from the Ministry of Education, Culture, Sports, Science and Technology as well as the Ministry of Health, Labor and Welfare of Japan.

References

[1] Lehmann-Horn F, Rudel R, Jurkat-rott K. Nondystrophic myotonias and periodic paralyses. In: Engel AG, Franzini-Armstrong C, editors. Myology. 3rd ed. New York: McGraw Hill; 2004. p. 1257–300.
[2] Matthews E, Fialho D, Tan SV, Venamce SL, Cannon SC, Sternberg D, et al. The non-dystrophic myotonicas: molecular pathogenesis, diagnosis and treatment. Brain 2010;133:9–12.
[3] Plassart E, Eymard B, Maurs L, Hauw JJ, Lyon-Caen O, Fardeau M. Paramyotonia congenita: genotype to phenotype correlations in two families and report of a new mutation in the sodium channel gene. J Neurol Sci 1996;142:126–33.
[4] Colding-Jorgensen E, Duno M, Vissing J. Autosomal dominant monosymptomatic myotonia premanens. Neurology 2006;67:153–5.
[5] Lerche BH, Heine R, Pika U, George Jr AL, Mitovic N, Browatzki M, et al. Human sodium channel myotonia: slowed channel inactivation due to substitutions for a glycine within the III-IV linker. J Physiol 1993;470:13–22.
[6] Rudel R, Ricker K, Lehmann-Horn F. Genotype–phenotype correlations in human skeletal muscle sodium channel diseases. Arch Neurol 1993;50:1241–8.
[7] Lion-Francois L, Mignot C, Vicart S, Manel V, Sternberg D, Landrieu P, et al. Severe neonatal episodic laryngospasm due to de novo SCN4A mutation. Neurology 2010;75:641–5.
[8] Gay S, Dupuis D, Faovre L, Masurel-Paulet A, Labenne M, Colombani M, et al. Severe neonatal non-dystrophic myotonia secondary to a novel mutation of the voltage-gated sodium channel (SCN4A) gene. Am J Med Genet A 2008;146:380–3.
[9] Goldin AL. Mechanisms of sodium channel inactivation. Curr Opin Neurobiol 2003;13(3):284–90.
[10] Hayward LJ, Sandoval GM, Cannnon SC. Defective slow inactivation of sodium channels contributes to familial periodic paralysis. Neurology 1999;52:1447–53.

Please cite this article as: Yoshinaga H, et al, A novel mutation in SCN4A causes severe myotonia and school-age-onset paralytic episodes, J Neurol Sci (2012), doi:10.1016/j.jns.2011.12.015

[11] Topaloglu BH, Serdaroglu A, Okan M, Gucuyener K, Tope M. Improvement of myotonia with carbamazepine in three cases with the Schwartz–Jampel syndrome. Neuropediatrics 1993;24:232–4.
[12] Fournier E, Arzel M, Sternberg D, Vicart S, Laforet P, Eymard B, et al. Electromyography guides toward subgroups of mutations in muscle channelopathies. Ann Neurol 2004;56:650–61.
[13] Fournier E, Viala K, Gervais H, Sternberg D, Arzel M, Vicart S, et al. Cold extends electromyography distinction between ion channel mutations causing myotonia. Ann Neurol 2006;60:356–65.
[14] Hayward LJ, Brown Jr RH, Cannon SC. Inactivation defects caused by myotonia-associated mutations in the sodium channel III–IV linker. J Gen Physiol 1996;107:559–76.
[15] Heatwole CR, Moxley III RT. The nondystrophic myotonia. Neurotherapeutics 2007;4:238–51.
[16] Plassart-Schiess E, Lhuillier L, George Jr AL, Fontaine B, Tabti N. Functional expression of the Ile693Thr Na+ channel mutation associated with paramyotonia congenital in a human cell line. J Physiol 1998;507(3):721–7.
[17] Takahashi MP, Cannon SC. Enhanced slow inactivation by V 445M: a sodium channel mutation associated with myotonia. Biophys J 1999;76:861–8.
[18] Bendahhou S, Cummins TR, Kula RW, Fu YH, Ptacek LJ. Impairment of slow inactivation as a common mechanism for periodic paralysis in DIIS4-S5. Neurology 2002;58:1266–72.

Please cite this article as: Yoshinaga H, et al, A novel mutation in SCN4A causes severe myotonia and school-age-onset paralytic episodes, J Neurol Sci (2012), doi:10.1016/j.jns.2011.12.015

Neuroscience Letters 519 (2012) 67–72

Contents lists available at SciVerse ScienceDirect

Neuroscience Letters

journal homepage: www.elsevier.com/locate/neulet

A sodium channel myotonia due to a novel *SCN4A* mutation accompanied by acquired autoimmune myasthenia gravis

Yosuke Kokunai[a], Keigo Goto[b], Tomoya Kubota[a], Takaaki Fukuoka[b], Saburo Sakoda[a,c], Tohru Ibi[d], Manabu Doyu[b], Hideki Mochizuki[a], Ko Sahashi[b], Masanori P. Takahashi[a,*]

[a] *Department of Neurology, Osaka University Graduate School of Medicine, Osaka, Japan*
[b] *Department of Neurology, Aichi Medical University School of Medicine, Japan*
[c] *Department of Neurology, National Hospital Organization Toneyama National Hospital, Japan*
[d] *Department of Pathophysiology and Therapeutics, Aichi Medical University School of Nursing, Japan*

HIGHLIGHTS

- Mutations of Na channel are known to be responsible for myotonia and myasthenia.
- A patient with non-dystrophic myotonia with acquired myasthenia was presented.
- A novel mutation G1292D was identified in the skeletal muscle Na channel.
- Consistently with myotonia, the mutant channel showed enhanced activation.
- Reduced use-dependent inactivation suggested opposing effect to myasthenia.

ARTICLE INFO

Article history:
Received 9 February 2012
Received in revised form 19 April 2012
Accepted 7 May 2012

Keywords:
Skeletal muscle
Myasthenia gravis
Electrophysiology
Patch clamp
Na channel
NaV1.4

ABSTRACT

Mutations of the voltage gated sodium channel gene (*SCN4A*) are responsible for non-dystrophic myotonia including hyperkalemic periodic paralysis, paramyotonia congenita, and sodium channel myotonia, as well as congenital myasthenic syndrome. *In vitro* functional analyses have demonstrated the non-dystrophic mutants to show a gain-of-function defect of the channel; a disruption of fast inactivation, an enhancement of activation, or both, while the myasthenic mutation presents a loss-of function defect. This report presents a case of non-dystrophic myotonia that is incidentally accompanied with acquired myasthenia. The patient presented a marked warm-up phenomenon of myotonia but the repeated short exercise test suggested mutations of the sodium channel. The genetic analysis identified a novel mutation, G1292D, of *SCN4A*. A functional study of the mutant channel revealed marked enhancement of activation and slight impairment of fast inactivation, which should induce muscle hyperexcitability. The effects of the alteration of channel function to the myasthenic symptoms were explored by using stimulation of repetitive depolarization pulses. A use-dependent channel inactivation was reduced in the mutant in comparison to normal channel, thus suggesting an opposing effect to myasthenia.

Myotonia, an abnormality of muscle relaxation, manifests in several non-dystrophic hereditary muscle diseases that are caused by genetic defect of the gene that codes for the voltage-gated sodium channel or chloride channel of skeletal muscle [9,12,17]. The myotonic phenotypes of the sodium channelopathies have been clinically classified as hyperkalemic periodic paralysis, paramyotonia congenita, and sodium channel myotonia (potassium-aggravated myotonia), based on symptoms like muscle paresis and myotonia [2,12,14]. More than 30 missense mutations responsible for non-dystrophic myotonia have been identified in the human skeletal muscle of the sodium channel α subunit gene (*SCN4A*) [2,12,17]. Functional analyses of the mutant sodium channels have revealed gain-of-function defects of the channel such as disruption of fast inactivation, enhanced activation, or both [2]. In addition, disruption of the slow inactivation is suggested to predispose patients to episodes of paralysis [1,8]. V1442E and possibly S246L mutations of *SCN4A* were identified in congenital myasthenic syndrome [16]. Unlike the mutations responsible for myotonia, these mutant channels show a loss-of-function defect.

The present study identified a novel mutation of *SCN4A* in a patient with non-dystrophic myotonia showing a marked warm-up phenomenon. In addition, he had acquired autoimmune myasthenia gravis. This study investigated the functional defect of the mutant channel using heterologously expressed channels in

* Corresponding author at: Department of Neurology, Osaka University Graduate School of Medicine, D4, 2-2, Yamadaoaka, Suita, Osaka 565-0871, Japan. Tel.: +81 6 6879 3571; fax: +81 6 6879 3579.
E-mail address: mtakahas@neurol.med.osaka-u.ac.jp (M.P. Takahashi).

0304-3940/$ – see front matter © 2012 Elsevier Ireland Ltd. All rights reserved.
http://dx.doi.org/10.1016/j.neulet.2012.05.023

cultured cells. Furthermore, the effects of the functional changes of the sodium channel on myasthenic symptoms were explored.

The proband was a 32-year-old male that had difficulty walking since he was 1 year old due to stiffness of the leg muscles. His family was not consanguineous and had no history of neuromuscular diseases. His parents noticed his poor motor performance based on muscle stiffness since early childhood. Blepharoptosis and impaired ocular movement as well as skeletal anomalies of the funnel breast and muscular hypertrophy were noted at 7 years of age. He was diagnosed with myasthenia gravis, because his serum was positive for anti-acetylcholine receptor (AChR) antibody. The ocular symptoms were alleviated with oral administration of cholinesterase inhibitor but the muscle stiffness was persistent. The blepharoptosis was improved by oral corticosteroid, but he felt aggravated muscle stiffness. He was treated with 300 mg/day of mexiletine hydrochloride, but it was ineffective.

An evaluation at 32 years of age showed hypertrophy of the truncal and proximal groups of muscles. Blepharoptosis and restricted bilateral ocular movement were present. Both grip and percussion myotonia and myotonia of the face/limb/truncal muscles were observed. Myotonia was reduced by repeated exercise (warm up phenomenon), and worsened by cooling. His muscle strength was normal. Positive anti-AChR binding antibody (1.0 nmol/l; $n < 0.2$ nmol/l) and negative anti-Musk antibody were noted.

Needle electromyography (EMG) was performed using a concentric recording needle with a sampling frequency of 10 Hz–10 kHz. The compound muscle action potentials (CMAPs) of the *abductor digiti minimi* were evoked by supramaximal stimulation of the ulnar nerve for 0.2 ms. The repeated short exercise test was performed as previously reported [5,6].

Muscle samples were obtained from the *intercostalis* and *biceps brachii* muscle during thymectomy for myasthenia gravis and were snap-frozen. Ten μm thick sections were stained by hematoxylin–eosin, myosin ATPase (pH 10.2, 4.6 and 4.2), cholinesterase and immunostaining of AChR, IgG and C3.

Informed consent was obtained from the patient using protocols approved by the Institutional Ethics Review Board. Genomic DNA was extracted from blood leukocytes. All exons of the *SCN4A* and *CLCN1* were amplified using the polymerase chain reaction (PCR), and the purified fragments of PCR products were sequenced using dideoxynucleotide chain termination in an automated DNA sequencer (ABI 3100; PE Applied Biosystems, California) [11].

A site-directed mutagenesis kit (QuikChange; Stratagene, California) was used to introduce the G1292D mutation in human skeletal muscle sodium channel expression construct pRc/CMV-hSkM1.

Cultures of human embryonic kidney (HEK) cells and their transient transfection were performed as described previously [15]. Plasmid cDNAs that encoded WT and mutant human sodium channel α subunits (1.25 μg/35-mm dish), human sodium channel β subunit (2.5 μg), and a CD8 marker (0.25 μg) were co-transfected using the calcium phosphate method. Transfection-positive cells were identified under the microscope by micro-beads attached to anti-CD8 antibody (Invitrogen). Sodium currents were measured using conventional whole-cell recording techniques at 2–3 days after transfection. Recordings were made at room temperature 22 °C by an amplifier (Axopatch 200B; Molecular Devices, California). Any cells with peak currents of <0.5 or >10 nA on step depolarization from −120 mV to −10 mV were excluded. The pipette internal solution contained: 105 mM CsF, 35 mM NaCl, 10 mM ethylene-glycol tetraacetic acid (EGTA), and 10 mM Cs-HEPES (pH 7.4). The bath solution contained: 140 mM NaCl, 4 mM KCl, 2 mM $CaCl_2$, 1 mM $MgCl_2$, 5 glucose, and 10 mM Na-HEPES (pH 7.4). We waited at least 10 min for equilibration after gaining access to the cells. Protocols employed to analyze channel gating were described previously [7] and are briefly described in the following section. Curve fitting was manually performed off-line using the Origin software package (Microcal LLC, Massachusetts). Conductance was calculated as $G_{(V)} = I_{peak\,(V)}/(V - E_{rev})$, where the reversal potential, E_{rev}, was measured experimentally for each cell. Voltage dependence on activation was quantified by fitting conductance measures to a Boltzmann function as $G_{(V)} = G_{max}/[1 + \exp(-(V - V_{1/2})/k)]$. Steady-state fast inactivation was fitted to a Boltzmann function calculated as $I/I_{max} = 1/[1 + \exp((V - V_{1/2})/k)]$, where $V_{1/2}$ is the half-maximum voltage and k is the slope factor. Steady-state slow inactivation was fitted to a Boltzmann function with the non-zero pedestal (S_0). Symbols with error bars indicate mean ± standard error of the mean (SEM). Statistical significance was determined using the unpaired t-test with Origin and values for $p < 0.05$ were considered to be significant.

Surface EMG showed prolonged muscle activity after voluntary contraction, which suggests an abnormality of muscle relaxation, myotonia (Fig. 1A). Needle EMG confirmed abundant myotonic discharges in all muscles examined (Fig. 1B). Nerve conduction studies including repetitive nerve stimulation study were normal. The repeated short exercised test was performed to discriminate between myotonia caused by either Na or Cl channel mutations. The amplitude of CMAP decreased after strenuous exercise, at room temperature (pattern I by Fournier et al.) and the manner of decrease was slightly altered by cooling [5,6] (Fig. 1C). This finding suggests a myotonic disorder caused by a Na channel mutation.

The muscle biopsy revealed the normal checker-board pattern of histochemical fiber types. The AChR stain was markedly attenuated at the motor endplate, and immune complexes of both IgG and C3 were positive, which is consistent with acquired autoimmune myasthenia gravis (AChR-MG) (Fig. 1D) [4].

No mutation was found in the *CLCN1* gene. An A-to-G translation was identified in the *SCN4A* gene (c. 3875 g > a G1292D) (Fig. 2A). This mutation was not found in any of more than 100 normal controls (data not shown). Glycine at amino acid position 1292 in Nav1.4, which is localized near the intracellular face of the segment S6 in domain III of the channel (Fig. 2B), is preserved among homologs in many species, including drosophila and zebra fish (Fig. 2C), and among orthologs of the voltage-gated sodium channel in brain, peripheral nerve, and heart in human (Nav1.1–1.9; data not shown).

The kinetics of sodium channel gating were examined by recording whole-cell sodium currents from HEK cells that express human skeletal muscle sodium channels. The current density of the mutant channel was approximately half that of the WT (WT: 443 ± 102 G1292D: 204 ± 43 pA/pF). Fig. 3A shows the current for WT and mutant channel normalized to the maximum amplitude, which are elicited by step depolarization pulses from a holding potential of −120 mV. The mutant channels were consistently activated at more hyperpolarized voltages than the WT channels, thus suggesting an enhanced activation.

Sodium conductance was calculated from the measured reversal potential, the mean of which was not significantly different between the WT and G1292D channels, and its voltage dependence is plotted in Fig. 3B. The midpoint of voltage dependence of activation was significantly shifted in the direction of hyperpolarization by 5.6 mV in G1292D in comparison to the WT (i.e. enhanced activation) (Table 1).

The G1292D current was also different from the WT with slower decay of macroscopic currents, suggesting an impaired fast inactivation (Fig. 3A). The voltage dependence of the steady-state fast inactivation was measured as the peak current elicited after a 300-ms conditioning pre-pulse from a holding potential of −120 mV. Although insignificant ($p = 0.052$), the midpoint of the steady-state inactivation curve for G1292D ($V_{1/2}$) was slightly shifted in the direction of depolarization in comparison to the WT

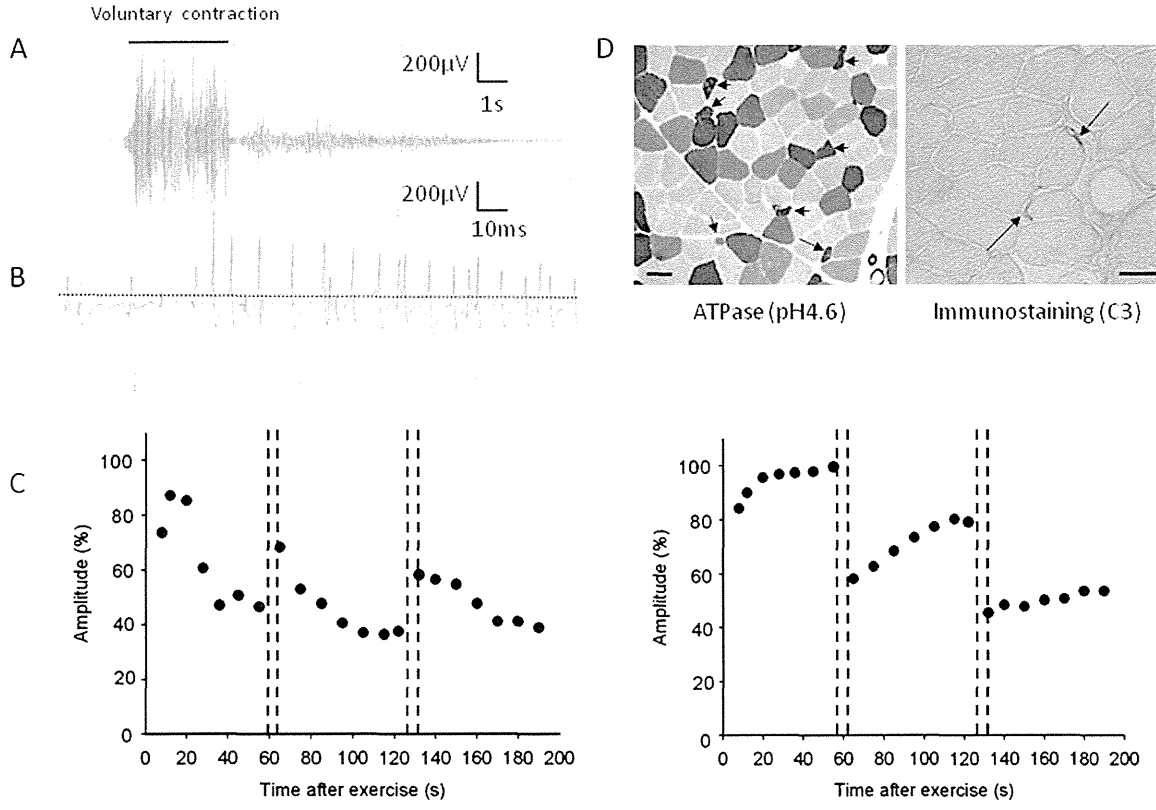

Fig. 1. Clinical electrophysiology and muscle pathology. (A) Myotonia was recorded with surface electromyography (EMG) as a continuous spontaneous activity after a voluntary contraction. (B) Needle EMG of the rectus femoris muscle revealed myotonic discharge. (C) Repeated short exercise tests at room temperature (left) and cooling (right) are shown. A gradual decrease of the amplitude of CMAPs was observed at room temperature. (D) Left: Biopsy from the *biceps brachii* muscle revealed normal checkerboard pattern of fiber types with actomyosin ATPase staining of pH 4.6. Arrows indicate type 1 fibers. Bar 20 μm. Right: The intercostal muscle biopsy. Immunostaining of complement 3 (C3) was positive at motor endplates (arrows). Bar 30 μm.

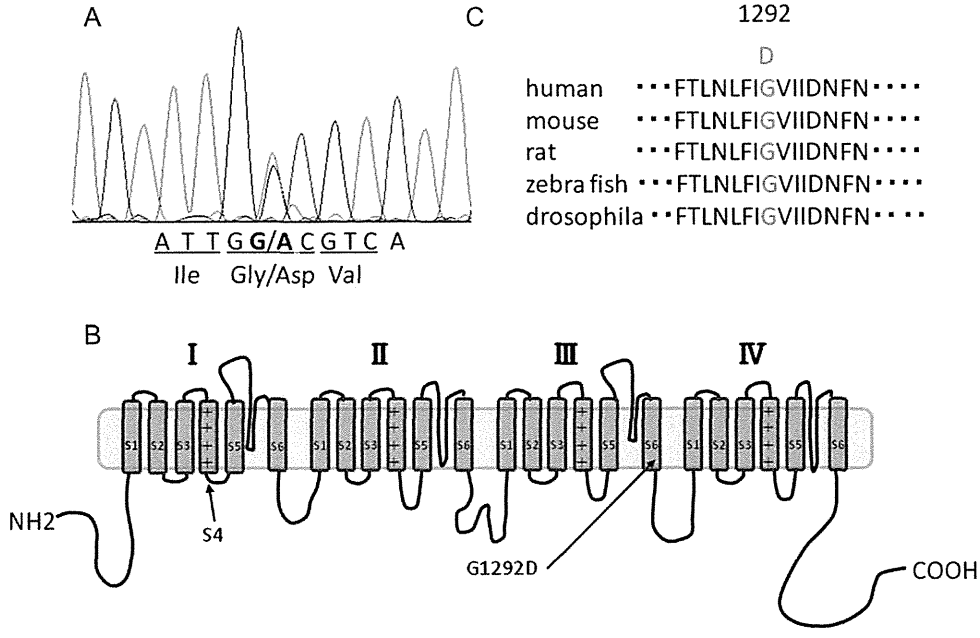

Fig. 2. A new mutation, G1292D, of the skeletal muscle sodium channel. (A) Nucleotide sequence analysis shows an A-to-G transition at nucleotide position 3875, resulting in the substitution of normal glycine by aspartic acid at amino acid position 1292 in Nav1.4 (G1292D). (B) Schematic illustration of the Nav1.4 channel. G1292D is located near the intracellular face of the segment S6 in domain III. (C) Glycine at amino acid position 1292 in Nav1.4 is preserved among homologs of many species.

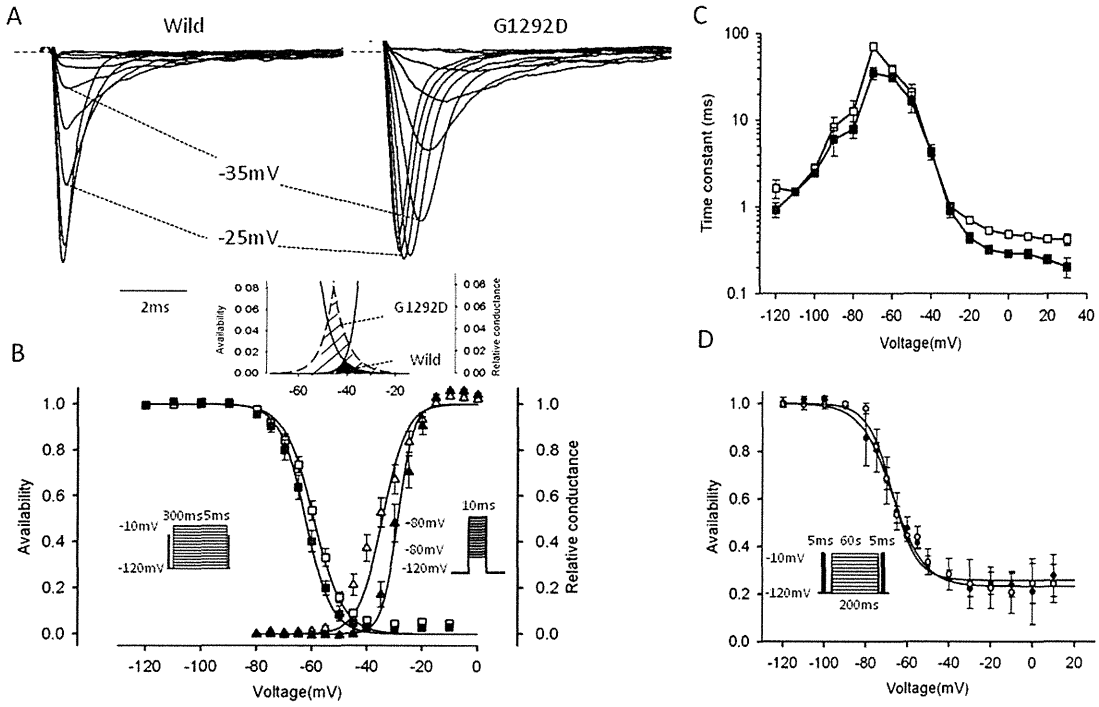

Fig. 3. The G1292D channel shows enhanced activation and slight impairment of fast inactivation. Filled symbols represent WT channel data. Open symbols show G1292D channel data. (A) Normalized currents for the WT and mutant channels, which are elicited by step depolarization pulses from a holding potential of −120 mV. The G1292D channels are activated at more hyperpolarized voltages than the WT channels. The G1292D channel also differs from the WT with slower decay of macroscopic currents. (B) Voltage dependence of availability (steady-state fast inactivation, left, squares) and conductance (activation, right, triangles) for WT and G1292D are shown. The midpoint of the activation curve for G1292D is shifted in the direction of hyperpolarization. The insets show the protocol used. An overlay of the WT and mutant window currents are also shown (top). (C) Voltage dependence of the kinetics of fast inactivation is shown by combining data from three different protocols: two-pulse recovery, two-pulse entry and single-pulse relaxation. The time constants for G1292D are slower than WT at the depolarized potential. (D) The voltage dependence of steady-state slow inactivation does not differ between G1292D and WT. The inset shows the protocol. A −10-mV test pulse is applied after a 60-s conditioning pre-pulse followed by a 20-ms gap at −120 mV to allow for the recovery from fast inactivation.

(Fig. 3B). Voltage-dependence of the conductance and the inactivation curves were magnified to illustrate voltage range at which channels activate but not fully inactivate, resulting in a small population of channels that conduct steady inward current known as window current. The area of the window current for G1292D was markedly increased compared to WT.

The kinetics of fast inactivation were characterized by quantifying the voltage dependence of the time constant with three different protocols. The time constants of fast inactivation in the depolarized range (−35 mV to +35 mV) were measured by fitting decay of the current elicited by step depolarization with a single exponential. The time constants in the depolarized range for G1292D were slower than in the WT (Fig. 3C). The time constants of fast inactivation at hyperpolarized potential (−120 mV to −80 mV) measured with the recovery protocol and those at intermediate voltages (−60 mV to −40 mV) measured using a two-pulse entry protocol were not significantly different. The slight depolarized shift in the $V_{1/2}$ of the steady-state inactivation (Fig. 3B) and slower rate of entry (Fig. 3C) suggests disrupted fast inactivation for the G1292D channel.

The voltage dependence of steady-state slow inactivation was measured as the peak current elicited by the test pulse after a 60-s conditioning pre-pulse followed by a 20-ms gap at −120 mV to allow recovery from fast inactivation (Fig. 3D, inset). The voltage dependence of slow inactivation and maximal extent of slow inactivation did not differ between the WT and G1292D (Table 1).

The response to a 5-Hz to 40-Hz train of 5-ms pulses was measured to assess whether the use-dependent Na channel inactivation affects myasthenic signs. Even in 5 Hz stimulation, the WT channel showed gradual decrease of the current. The changes were more evident in high-frequency stimulation. The normalized peak current amplitude at 250th pulse had a drop of only 4.8% for G1292D at 40 Hz stimulation, whereas the WT showed a 9.6% decrease (Fig. 4).

This report presented a case of non-dystrophic myotonia accompanied with unambiguous evidence of AChR-MG. A novel mutation, G1292D, was identified in the voltage-gated sodium channel of skeletal muscle. The *in vitro* functional study of the mutant channel has revealed significantly enhanced activation or destabilized closed state, and slight impairment of fast inactivation; both should induce hyperexcitability of the skeletal muscle membrane.

Table 1
Parameter estimates for G1292D and WT.

	Activation		Fast inactivation		Slow inactivation		
	$V_{1/2}$ (mV)	k (mV/e-fold)	$V_{1/2}$ (mV)	k (mV/e-fold)	$V_{1/2}$ (mV)	k (mV/e-fold)	S_0
WT	−28.9 ± 1.3 (15)	2.8 ± 0.2 (15)	−62.4 ± 1.1 (15)	4.8 ± 0.2 (15)	−67.4 ± 2.3 (3)	6.1 ± 0.9 (3)	0.26 ± 0.08 (3)
G1292D	−34.5 ± 1.5 (24)*	4.4 ± 0.3 (24)*	−59.3 ± 1.0 (24)	5.3 ± 0.2 (24)	−67.1 ± 3.1 (3)	7.7 ± 1.1 (3)	0.23 ± 0.04 (3)

$V_{1/2}$ is the midpoint value of the steady-state inactivation curve and the voltage dependence of the conductance curve; k is the slope factor; S_0 is the non-zero pedestal of slow inactivation. Values are expressed as the mean ± SEM. Numbers in parenthesis indicate the number of recorded cells.

* Significant difference in comparison to WT ($p < 0.05$).

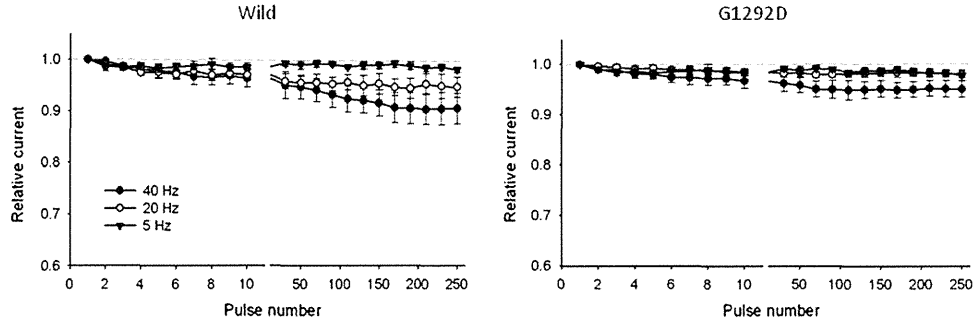

Fig. 4. The G1292D channel shows less use-dependent inactivation with repetitive stimulation. Relative Na current during a train of 5-ms depolarization to −10 mV from a holding potential of −100 mV are shown. Every 20th response is shown after the break at the 10th pulse (n = 5–7).

It is often possible to distinguish chloride from sodium channel myotonias based on the clinical features, but some cases of sodium channel myotonia exhibit clinical features that are very similar to those seen in myotonia congenita [18,19]. The present patient showed a marked warm-up phenomenon with slight worsening with cold stimuli suggestive of chloride channel myotonia. Exercise tests are reported to be helpful to distinguish from myotonias due to sodium or chloride channel mutation [5,6,12]. The patient presented a gradual and prolonged decrement in CMAP after short exercise even at normal temperature (pattern I by Fournier et al.). This pattern with a short exercise test suggests myotonia with sodium channel mutations, especially in those showing paramyotonia congenita. According to the CINCH classification, he should be classified as sodium channel myotonia, not paramyotonia congenita, since no paralytic attacks had been experienced. An additional study might be needed to clarify whether the exercise tests can predict the precise genotype.

The association between myotonia caused by a sodium channel mutation and the AChR-MG should be discussed. At least two features which are caused by the mutations of Na channel might have ameliorated the myasthenic phenotype of the patient. First, the presence of the marked warm up phenomenon might mask the fatigability of the patient. Although the mechanism is not well understood, a warm up phenomenon, which is defined as alleviation of muscle stiffness with repetition of the exercise, is frequently observed in myotonia congenita due to Cl channel mutations but is also reported for some patients with Na channel myotonia [3].

Next, the reduction of use-dependent inactivation on high-frequency stimulation, observed in mutant channel expressed *in vitro*, might also ameliorate the myasthenic features. In contrast to the current case, an enhanced use-dependent inactivation on high-frequency stimulation is observed in V1442E, a mutation responsible for congenital myasthenic syndrome. The enhanced use-dependent inactivation in the V1422E channel is attributed to a markedly enhanced fast inactivation of the mutant channel. Further cases and studies are necessary but this rare case raises an interesting question regarding the relation of myotonic and myasthenic features. It should also be pointed out that a decrease of CMAP amplitude after repetitive nerve stimulation is usually observed in myotonic patients, especially in myotonia congenita.

G1292D is the second mutation located near the intracellular face of the segment S6 in domain III of the sodium channel protein that has been identified. The previously identified mutation, V1293I, which is located next to the current mutation, is similar to the current case. Clinically the patient presented myotonia with a warm up phenomenon and no paralytic attack [10]. Electrophysiology shows that fast inactivation is just barely perturbed, the voltage dependence of activation is significantly shifted to the hyperpolarized direction and no abnormality is observed in slow inactivation [7]. Both mutations, located near the intracellular mouth of the ion conducting pore, could affect fast inactivation mediated by docking of the interdomain III–IV linker [20]. Another possibility is the mutation affects coupling between voltage sensor and pore, since a scanning tryptophan mutagenesis study of rat channel shows that mutation of the residue corresponding to V1293 causes the voltage sensor to activate more easily while concurrently making the opening of the pore more difficult [13].

We identified a novel mutation, G1292D, of *SCN4A* in a non-dystrophic myotonia with acquired myasthenia. Our studies show that functional change of the mutant channel was consistent with myotonia but had opposing effect to myasthenia.

Acknowledgments

This study was supported partly by Research Grants from the Ministry of Health, Labour and Welfare, Intramural research grant (23-5) of NCNP and grants-in-aid from JSPS (to MPT).

References

[1] S. Bendahhou, T.R. Cummins, R.W. Kula, Y.H. Fu, L.J. Ptacek, Impairment of slow inactivation as a common mechanism for periodic paralysis in DIIS4-S5, Neurology 58 (2002) 1266–1272.
[2] S.C. Cannon, Pathomechanisms in channelopathies of skeletal muscle and brain, Annual Review of Neuroscience 29 (2006) 387–415.
[3] N. Dupre, N. Chrestian, J.P. Bouchard, E. Rossignol, D. Brunet, D. Sternberg, B. Brais, J. Mathieu, J. Puymirat, Clinical, electrophysiologic, and genetic study of non-dystrophic myotonia in French-Canadians, Neuromuscular Disorders 19 (2009) 330–334.
[4] A.G. Engel, K. Sahashi, G. Fumagalli, The immunopathology of acquired myasthenia gravis, Annals of the New York Academy of Sciences 377 (1981) 158–174.
[5] E. Fournier, M. Arzel, D. Sternberg, S. Vicart, P. Laforet, B. Eymard, J.C. Willer, N. Tabti, B. Fontaine, Electromyography guides toward subgroups of mutations in muscle channelopathies, Annals of Neurology 56 (2004) 650–661.
[6] E. Fournier, K. Viala, H. Gervais, D. Sternberg, M. Arzel-Hezode, P. Laforet, B. Eymard, N. Tabti, J.C. Willer, C. Vial, B. Fontaine, Cold extends electromyography distinction between ion channel mutations causing myotonia, Annals of Neurology 60 (2006) 356–365.
[7] D.S. Green, A.L. George Jr., S.C. Cannon, Human sodium channel gating defects caused by missense mutations in S6 segments associated with myotonia: S804F and V1293I, Journal of Physiology 510 (Pt 3) (1998) 685–694.
[8] L.J. Hayward, G.M. Sandoval, S.C. Cannon, Defective slow inactivation of sodium channels contributes to familial periodic paralysis, Neurology 52 (1999) 1447–1453.
[9] C.R. Heatwole, R.T. Moxley 3rd, The nondystrophic myotonias, Neurotherapeutics 4 (2007) 238–251.
[10] M.C. Koch, K. Baumbach, A.L. George, K. Ricker, Paramyotonia congenita without paralysis on exposure to cold: a novel mutation in the SCN4A gene (Val1293Ile), Neuroreport 6 (1995) 2001–2004.
[11] T. Kubota, X. Roca, T. Kimura, Y. Kokunai, I. Nishino, S. Sakoda, A.R. Krainer, M.P. Takahashi, A mutation in a rare type of intron in a sodium-channel gene results in aberrant splicing and causes myotonia, Human Mutation 32 (2011) 773–782.
[12] E. Matthews, D. Fialho, S.V. Tan, S.L. Venance, S.C. Cannon, D. Sternberg, B. Fontaine, A.A. Amato, R.J. Barohn, R.C. Griggs, M.G. Hanna, The non-dystrophic myotonias: molecular pathogenesis, diagnosis and treatment, Brain 133 (2010) 9–22.
[13] Y. Muroi, M. Arcisio-Miranda, S. Chowdhury, B. Chanda, Molecular determinants of coupling between the domain III voltage sensor and pore of a sodium channel, Nature Structural Molecular Biology 17 (2010) 230–237.
[14] R. Rudel, F. Lehmann-Horn, Paramyotonia, potassium-aggravated myotonias and periodic paralyses, in: 37th ENMC International Workshop, Naarden,

the Netherlands, 8–10 December 1995, Neuromuscular Disord 7 (1997) 127–132.
[15] M.P. Takahashi, S.C. Cannon, Enhanced slow inactivation by V445M: a sodium channel mutation associated with myotonia, Biophysical Journal 76 (1999) 861–868.
[16] A. Tsujino, C. Maertens, K. Ohno, X.M. Shen, T. Fukuda, C.M. Harper, S.C. Cannon, A.G. Engel, Myasthenic syndrome caused by mutation of the SCN4A sodium channel, Proceedings of the National Academy of Sciences of the United States of America 100 (2003) 7377–7382.
[17] S. Vicart, D. Sternberg, B. Fontaine, G. Meola, Human skeletal muscle sodium channelopathies, Neurological Sciences 26 (2005) 194–202.
[18] B. Wakeman, D. Babu, J. Tarleton, I.M. Macdonald, Extraocular muscle hypertrophy in myotonia congenita, Journal of AAPOS 12 (2008) 294–296.
[19] B. Wakeman, I.M. MacDonald, I. Ginjaar, J. Tarleton, D. Babu, Extraocular muscle hypertrophy in myotonia congenita: mutation identified in the SCN4A gene (V445M), Journal of AAPOS 13 (2009) 526–527.
[20] J.W. West, D.E. Patton, T. Scheuer, Y. Wang, A.L. Goldin, W.A. Catterall, A cluster of hydrophobic amino acid residues required for fast Na(+)-channel inactivation, Proceedings of the National Academy of Sciences of the United States of America 89 (1992) 10910–10914.

ARTICLE IN PRESS
MATBIO-00900; No of Pages 12
Matrix Biology xxx (2012) xxx–xxx
Contents lists available at SciVerse ScienceDirect
Matrix Biology
journal homepage: www.elsevier.com/locate/matbio

Perlecan modulates VEGF signaling and is essential for vascularization in endochondral bone formation

Muneaki Ishijima [a,b], Nobuharu Suzuki [a], Kentaro Hozumi [a], Tomoya Matsunobu [a], Keisuke Kosaki [a], Haruka Kaneko [b], John R. Hassell [c], Eri Arikawa-Hirasawa [d], Yoshihiko Yamada [a,*]

[a] Laboratory of Cell and Developmental Biology, National Institute of Dental and Craniofacial Research, National Institutes of Health, Bethesda, Maryland 20892-4370, USA
[b] Department of Medicine for Motor Organs, Juntendo University Graduate School of Medicine, Tokyo 113-8421, Japan
[c] Department of Molecular Medicine, College of Medicine, University of South Florida, Tampa, FL 33612-4799, USA
[d] Research Institute for Diseases of Old Age, Juntendo University Graduate School of Medicine, Tokyo 113-8421, Japan

ARTICLE INFO

Article history:
Received 30 November 2011
Received in revised form 27 February 2012
Accepted 28 February 2012
Available online xxxx

Keywords:
Perlecan
Endochondral bone formation
Growth plate
Vascular invasion
VEGF signaling

ABSTRACT

Perlecan (Hspg2) is a heparan sulfate proteoglycan expressed in basement membranes and cartilage. Perlecan deficiency ($Hspg2^{-/-}$) in mice and humans causes lethal chondrodysplasia, which indicates that perlecan is essential for cartilage development. However, the function of perlecan in endochondral ossification is not clear. Here, we report the critical role of perlecan in VEGF signaling and angiogenesis in growth plate formation. The $Hspg2^{-/-}$ growth plate was significantly wider but shorter due to severely impaired endochondral bone formation. Hypertrophic chondrocytes were differentiated in $Hspg2^{-/-}$ growth plates; however, removal of the hypertrophic matrix and calcified cartilage was inhibited. Although the expression of MMP-13, CTGF, and VEGFA was significantly upregulated in $Hspg2^{-/-}$ growth plates, vascular invasion into the hypertrophic zone was impaired, which resulted in an almost complete lack of bone marrow and trabecular bone. We demonstrated that cartilage perlecan promoted activation of VEGF/VEGFR by binding to the VEGFR of endothelial cells. Expression of the perlecan transgene specific to the cartilage of $Hspg2^{-/-}$ mice rescued their perinatal lethality and growth plate abnormalities, and vascularization into the growth plate was restored, indicating that perlecan in the growth plate, not in endothelial cells, is critical in this process. These results suggest that perlecan in cartilage is required for activating VEGFR signaling of endothelial cells for vascular invasion and for osteoblast migration into the growth plate. Thus, perlecan in cartilage plays a critical role in endochondral bone formation by promoting angiogenesis essential for cartilage matrix remodeling and subsequent endochondral bone formation.

Published by Elsevier B.V.

1. Introduction

Most bones, such as the long bones, are formed by endochondral ossification, in which cartilage during growth is first formed as a template and then replaced by bone (Karsenty, 2003; Kronenberg, 2003). Endochondral ossification is initiated by the condensation of mesenchymal cells, which differentiate into chondrocytes. The cells surrounding the mesenchyme condensation differentiate into the perichondrium. Proliferating chondrocytes produce a large number of matrix molecules, such as collagen II and aggrecan, to expand the cartilage template, cease proliferation at the prehypertrophic zone in the middle of the growth plate, and further differentiate into collagen X-expressing hypertrophic chondrocytes. The matrix surrounding mature hypertrophic chondrocytes is mineralized and replaced with osteoblasts. Although cartilage is a neovascular tissue, factors such as vascular endothelial growth factor (VEGF) produced by hypertrophic chondrocytes induce vascular invasion into the perichondrium and cartilage near the terminal region of the cartilage template, which is required for cartilage matrix remodeling and osteoblast migration from the perichondrium for ossification and bone marrow formation (Zelzer et al., 2004). This indicates that endochondral bone formation is a process highly coordinated between chondrogenesis and osteogenesis.

Perlecan plays critical roles in normal development, tissue functions, and diseases (Olsen, 1999; DeCarlo and Whitelock, 2006; Knox and Whitelock, 2006; Zoeller et al., 2009). Perlecan is a proteoglycan present in all basement membranes and other tissues, such as cartilage, plays important roles in development and tissue functions, and is associated with various diseases (Olsen, 1999; Morita et al., 2005; DeCarlo and Whitelock, 2006; Knox and Whitelock, 2006; Zoeller et al., 2009). Perlecan consists of a large elongated core protein with a complex modular structure and is usually substituted with several heparan sulfate and/or chondroitin sulfate chains (Noonan et al.,

* Corresponding author at: Bldg. 30, Rm. 407, NIDCR, NIH, 30 Convent Drive MSC 4370, Bethesda, MD 20892-4370, USA. Tel.: +1 301 496 2111; fax: +1 301 402 0897.
E-mail address: yoshi.yamada@nih.gov (Y. Yamada).

0945-053X/$ – see front matter. Published by Elsevier B.V.
doi:10.1016/j.matbio.2012.02.006

1991). Perlecan binds basement membrane components, such as laminins and collagen IV, providing scaffolding for cells in many tissues and creating a barrier to the passage of molecules in the kidneys (Hopf et al., 1999; Morita et al., 2005). Perlecan also binds other extracellular proteins, such as fibronectin and fibulin. Perlecan modulates cell proliferation and differentiation through interaction with cell surface receptors such as integrins and with growth factors such as FGFs (Aviezer et al., 1994; Brown et al., 1997). Many biological functions of perlecan have been reported, such as aiding supramolecular organization of basement membranes and cell-matrix interactions (Brown et al., 1997; Hopf et al., 1999; Kvist et al., 2006), storage and release of various cytokines (Klein et al., 1995; Whitelock et al., 1996; Ghiselli et al., 2001; Govindraj et al., 2006; Smith et al., 2007), control of extracellular proteolysis and macromolecular filtration (Mongiat et al., 2003; Morita et al., 2005), and angiogenesis (Aviezer et al., 1994; Jiang and Couchman, 2003; Segev et al., 2004; Zhou et al., 2004).

Studies in knockout mice and mutations in the perlecan gene (HSPG2) in humans revealed that perlecan is essential for cartilage development (Arikawa-Hirasawa et al., 1999; Costell et al., 1999; Arikawa-Hirasawa et al., 2001a,b). Perlecan knockout (Hspg2$^{-/-}$) mice develop severe skeletal dysplasia characterized by shortened bones and craniofacial abnormalities and die shortly after birth of respiratory failure due to the cartilage defects of the rib cage (Arikawa-Hirasawa et al., 1999; Costell et al., 1999). Proliferation of chondrocytes is reduced in Hspg2$^{-/-}$ mice (Arikawa-Hirasawa et al., 1999). The cartilage matrix of the knockout mice contains disorganized collagen fibrils and glycosaminoglycans, which suggests that perlecan plays an important role in the cartilage matrix structure (Kvist et al., 2006). A human disorder, dyssegmental dysplasia, Silverman-Handmaker type (DDSH), was identified as a functional null mutation of perlecan and causes skeletal abnormalities similar to those of the knockout mice (Arikawa-Hirasawa et al., 2001a,b). In addition, subtle functional mutations of perlecan cause Schwartz-Jampel Syndrome (SJS), a rare autosomal recessive osteochondrodysplasia associated with myotonia (Nicole et al., 2000; Arikawa-Hirasawa et al., 2002; Rodgers et al., 2007). Patients with SJS survive and show much milder skeletal dysplasia compared to those with DDSH. We also showed that perlecan is critical for maintaining fast muscle mass and fiber composition by regulating myostatin signaling

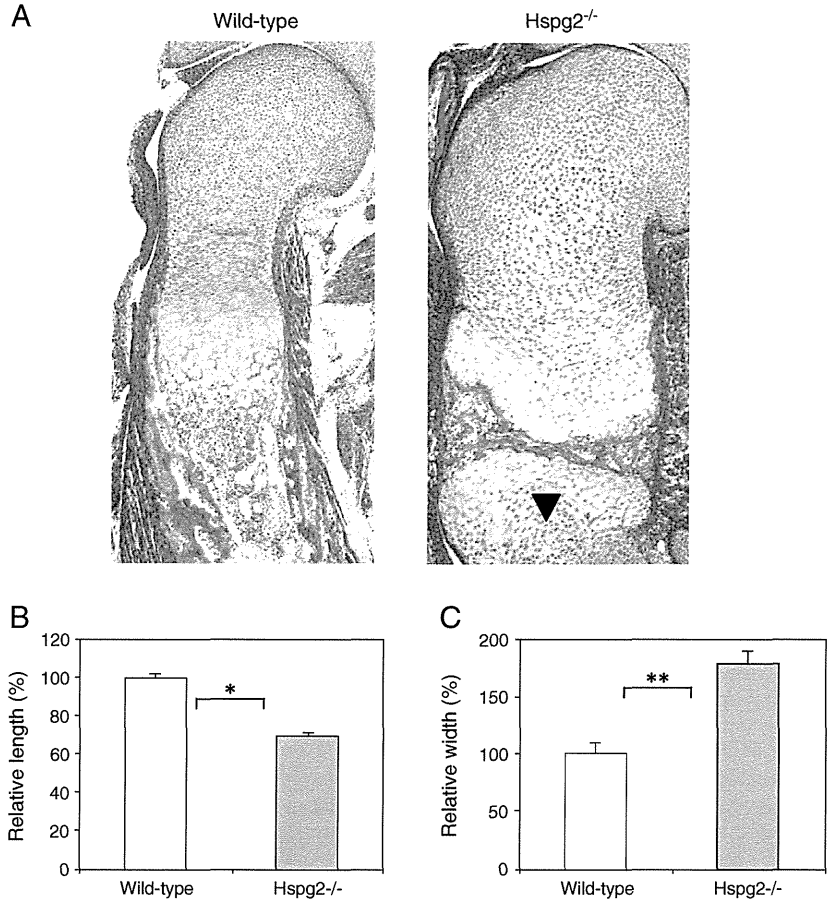

Fig. 1. Endochondral ossification was impaired in the growth plate of Hspg2$^{-/-}$ mice. (A) H-E staining of the proximal end of the humerus in E16.5 wild-type and Hspg2$^{-/-}$ mice. The long bones of Hspg2$^{-/-}$ mice were shorter than those of wild-type mice, as the distal end of the growth plate (arrowhead) was observed in Hspg2$^{-/-}$ mice but not in wild-type mice. (B) Comparison of the humeral length of Hspg2$^{-/-}$ mice with that of wild-type mice. The relative length of the humerus in wild-type mice was set at 100%. * indicates $p<0.05$. **(C)** Comparison of the humeral width of Hspg2$^{-/-}$ mice with that of wild-type. The relative width of the humerus in wild-type mice was set at 100%. **Indicates $p<0.01$. **(D)** Double staining of Safranin-O (red) and von Kossa (brown) staining of the proximal end of the humerus at E16.5 in wild-type and Hspg2$^{-/-}$ mice. Reduced glycosaminoglycan levels in the growth plate of Hspg2$^{-/-}$ mice were observed compared with those of wild-type mice. In the growth plates of wild-type mice, the terminal hypertrophic zone was replaced with trabecular bone, and the perichondrium formed bone collars by membranous ossification. The bone collar aligns parallel to the longitudinal axis of the limb. In Hspg2$^{-/-}$ mice, levels of the calcified matrix in the terminal cartilage template were increased, and levels in the trabecular bone were reduced. Boxed areas are enlarged and shown below. (For interpretation of the references to color in this figure legend, the reader is referred to the web version of this article.)

Please cite this article as: Ishijima, M., et al., Perlecan modulates VEGF signaling and is essential for vascularization in endochondral bone formation, Matrix Biology (2012), doi:10.1016/j.matbio.2012.02.006

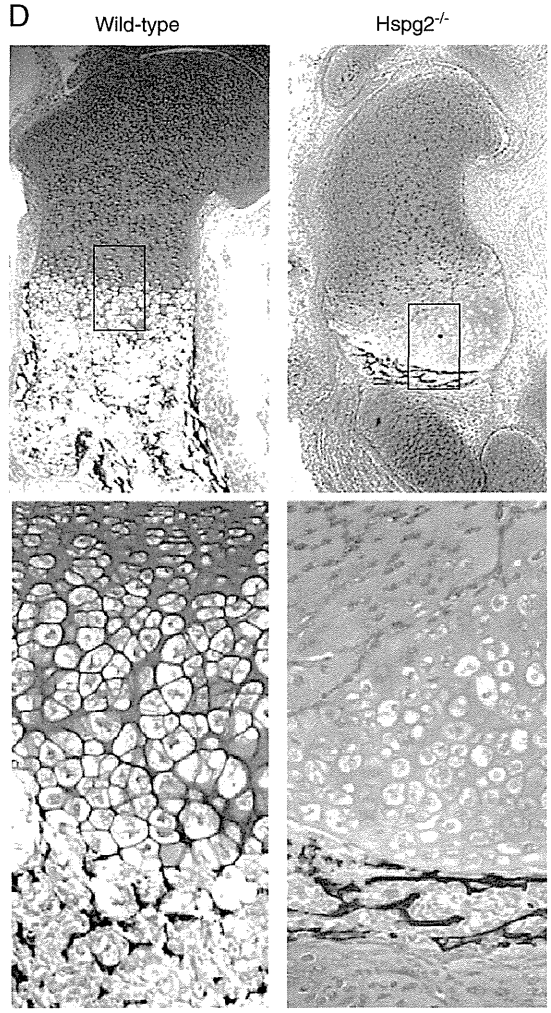

Fig. 1 (*continued*).

using lethality-rescued Hspg2$^{-/-}$-Tg mice by expressing recombinant perlecan specifically in the cartilage of the perlecan-null (Hspg2$^{-/-}$) genetic background (Xu et al., 2010), where perlecan is expressed in cartilage but absent in muscle, endothelial basement membranes, and other tissues.

Although perlecan plays a critical role in growth plate development, the function of perlecan in endochondral ossification is not clear. Here we analyzed the growth plates of Hspg2$^{-/-}$ and Hspg2$^{-/-}$-Tg mice and demonstrated that perlecan in cartilage, not in endothelial basement membranes, is required for vascular invasion and cartilage matrix remodeling that is essential for the formation of the trabecular bone and bone marrow.

2. Results

2.1. Endochondral ossification is inhibited in the growth plate of Hspg2$^{-/-}$ mice

Perlecan is essential for cartilage development, as perlecan deficiency in mice displays perinatal lethal chondrodysplasia (Arikawa-Hirasawa et al., 1999; Costell et al., 1999). In humans, null mutations of perlecan cause severe chondrodysplasia and DDSH, similar to Hspg2$^{-/-}$ mice. The humeri of E16.5 Hspg2$^{-/-}$ mice were shorter and wider than those of wild-type mice (Fig. 1A). Quantification analyses revealed that the humeri of Hspg2$^{-/-}$ mice were significantly shorter (Fig. 1B) and wider (Fig. 1C) compared to those of wild-type mice. The humeri of Hspg2$^{-/-}$ mice contained reduced levels of glycosaminoglycan, as shown with Safranin-O staining (Fig. 1D, red) and as described previously (Arikawa-Hirasawa et al., 1999; Costell et al., 1999). The striking abnormality of the growth plate of mutant mice is the almost complete lack of bone marrow cavities and trabecular bone (Fig. 1). In the E16.5 growth plates of wild-type mice, von Kossa staining (brown) showed that bone collar and trabecular bone were formed, and calcification of the matrix surrounding mature hypertrophic chondrocytes, as well as of the matrix surrounding the periosteum (bone collar) and trabecular bone, was observed (Fig. 1D). In contrast, in Hspg2$^{-/-}$ mice, thin calcified layers were observed along the bottom border of the cartilage and separated two cartilage regions, which were located close together in the almost complete absence of bone marrow.

2.2. Defect of perlecan in chondrocytes inhibits vascular invasion into the hypertrophic chondrocyte

The inhibition of the formation of bone marrow and trabecular bone suggests a defect in angiogenesis in the hypertrophic zone in Hspg2$^{-/-}$ growth plates. Therefore, we examined vascular invasion into the hypertrophic zone. Immunostaining of CD31 (PCAM-1), a marker of endothelial cells, showed that endothelial cells invaded cartilage from surrounding tissues, including the perichondrium and bone marrow, in wild-type mice (Fig. 2A). The chondro-osseous region was arranged perpendicularly to the long axis of the bone (Fig. 2A) in wild-type mice. In Hspg2$^{-/-}$ mice, bone marrow was almost completely absent, and CD31-positive endothelial cells (black) were observed in the perichondrium/periosteum and surrounding tissues (Fig. 2A). In addition, the proximal and distal cartilage areas were separated by thin calcified layers in the humeri of the Hspg2$^{-/-}$ mice (Figs. 1A, B, and 2A). These results suggest that vascular invasion into the hypertrophic zone from the surrounding tissues was severely inhibited in the absence of perlecan. TRAP-positive osteoclasts with multiple nuclei, which are differentiated from hematopoietic stem cells, migrated into the cartilage-bone interface and trabecular bone through the vasculature in wild-type mice (Fig. 2B). TRAP-positive osteoclasts (dark red) were present, but their numbers were reduced in the bone collar and surrounding region of the Hspg2$^{-/-}$ growth plates (Fig. 2B). These results further indicate that vascular invasion into the growth plate is impaired in Hspg2$^{-/-}$ mice.

2.3. VEGFA expression is increased in chondrocytes of Hspg2$^{-/-}$ mice

Vascular invasion is a crucial step in removing the cartilage matrix for endochondral ossification. VEGFA plays an important role in vascular invasion for endochondral ossification (Maes et al., 2002; Zelzer et al., 2002; Maes et al., 2004; Zelzer et al., 2004). Therefore, we examined the VEGFA protein expression level in chondrocytes in HSPG2$^{-/-}$ mice with immunostaining and confirmed with Western blot (Fig. 3). In Hspg2$^{-/-}$ mice, the expression levels of VEGFA proteins in hypertrophic chondrocytes were substantially increased compared with the control mice (Fig. 3A). Consistent with this immunostaining result, Western blotting revealed that VEGFA protein levels in the Hspg2$^{-/-}$ growth plate were increased compared to those in the wild-type growth plate (Fig. 3B).

2.4. VEGF$_{164}$ expression is increased in chondrocytes of Hspg2$^{-/-}$ mice

VEGFA consists of three splice variants, VEGF$_{120}$, VEGF$_{164}$, and VEGF$_{188}$ (Ruhrberg et al., 2002). Although VEGF$_{120}$, which does not have a heparan sulfate binding site in the C-terminal region, is important for vascular invasion in the epiphysis of the growth plate to form

Please cite this article as: Ishijima, M., et al., Perlecan modulates VEGF signaling and is essential for vascularization in endochondral bone formation, Matrix Biology (2012), doi:10.1016/j.matbio.2012.02.006

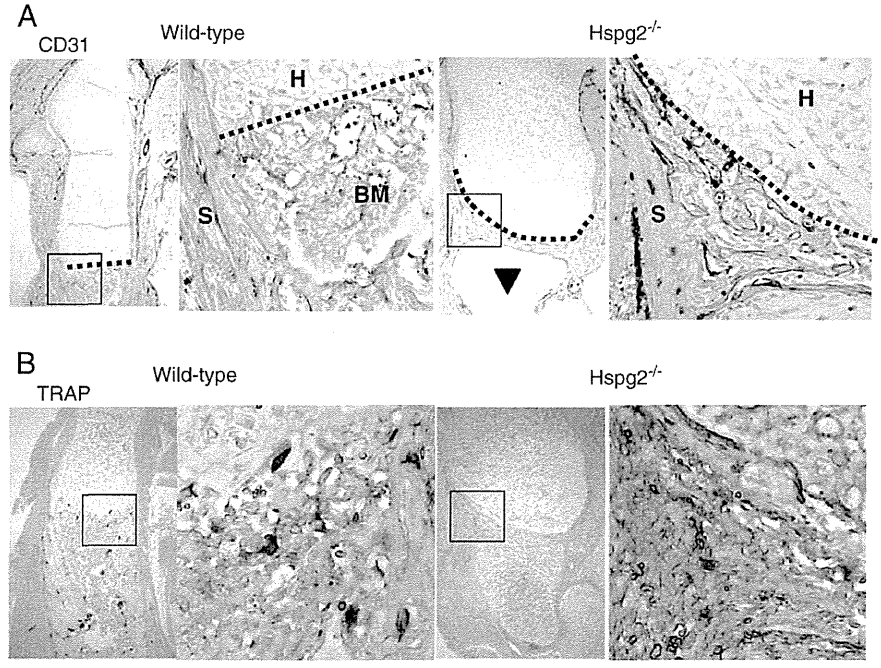

Fig. 2. Vascular invasion into the hypertrophic zone is inhibited in Hspg2$^{-/-}$ mice. (A) Immunostaining of CD31 (PCAM-1) (black) shows that endothelial cells invaded the chondro-osseous boundary and bone marrow from surrounding tissues in wild-type mice. Dotted line, chondro-osseous boundary; bone marrow (BM); hypertrophic zone (H); surrounding tissues (S). The dotted line in the growth plates of Hspg2$^{-/-}$ mice indicates the boundary between the hypertrophic zone and the abnormally curved perichondrium layer and bone collar surrounding the terminal hypertrophic zone. (B) Osteoclast differentiation was inhibited in the growth plates of Hspg2$^{-/-}$ mice. Multinucleated TRAP-positive osteoclasts (dark red) were observed in the chondro-osseous boundary as well as bone marrow in wild-type mice. In Hspg2$^{-/-}$ mice, TRAP-positive osteoclast numbers are lower in the boundary. (For interpretation of the references to color in this figure legend, the reader is referred to the web version of this article.)

the secondary ossification center (Maes et al., 2004), $VEGF_{164}$, which contains one of the two heparan sulfate binding sites, is critical for vascular invasion to form trabecular bone in the growth plate (Zelzer et al., 2004). We examined the mRNA expression levels of these isoforms of VEGFA in the growth plate chondrocytes in Hspg2$^{-/-}$ mice. Although two VEGF mRNA isoforms were expressed in chondrocytes prepared from the growth plates of wild-type mice, the expression levels of $VEGF_{164}$ were more dominant than those of $VEGF_{120}$ (Fig. 4A). In Hspg2$^{-/-}$ mice, these VEGF mRNA were also expressed, but their expression levels were found to be increased further than those in wild-type mice by using semi-quantitative RT-PCR analysis (Fig. 4A). Real-time PCR analysis of the expression levels of these three isoforms showed that, although these isoforms of VEGF mRNA were significantly increased in chondrocytes of Hspg2$^{-/-}$ mice compared to those of wild-type mice, the $VEGF_{164}$ mRNA levels were most profoundly increased in the absence of perlecan (Fig. 4B). These results indicate that the VEGFA expression level was not a major cause of the defect in vascular invasion into the growth plate cartilage of Hspg2$^{-/-}$ mice.

2.5. Expression of CTGF, Chm-1, and MMPs in the hypertrophic chondrocytes of Hspg2$^{-/-}$ mice

In addition to VEGFA, connective tissue growth factor (CTGF) plays an important role in vascular invasion in endochondral ossification. The absence of CTGF impairs vascular invasion (Ivkovic et al., 2003), while the absence of chondromodulin-1 (Ch-1) in vivo does not impair vascular invasion (Brandau et al., 2002). We found that the CTGF and Ch-1 mRNA levels in Hspg2$^{-/-}$ mice were significantly increased compared with those of the wild-type mice (Fig. 5A, B). Matrix metalloproteinases (MMPs) are also important for vascular invasion, as MMPs degrade most components of the extracellular matrix (ECM) that allow promotion of sprouting and migration of endothelial cells (Noel et al., 2004; Sottile, 2004). We found that the MMP13 mRNA levels were significantly increased in the growth plates of Hspg2$^{-/-}$ mice compared with those of wild-type mice (Fig. 5C). MMP-9 is also expressed in the hypertrophic chondrocytes of wild-type mice and Hspg2$^{-/-}$ mice (data not shown)(Gustafsson et al., 2003). These results indicate that the inhibition of vascular invasion in the growth plates of Hspg2$^{-/-}$ mice was not due to the reduced expression levels of CTGF and MMP.

2.6. Removal of hypertrophic matrix is inhibited in the absence of perlecan

We examined cartilage calcification and osteopontin (OPN) expression in E18.5 Hspg2$^{-/-}$ growth plates. Type X collagen expression was observed in Hspg2$^{-/-}$ mice (data not shown), as reported previously, although its expression levels are decreased in Hspg2$^{-/-}$ mice compared with those in wild-type mice (Arikawa-Hirasawa et al., 1999; Costell et al., 1999). At E18.5, formation of hydroxyapatite nodules (calcospherites) was observed in the hypertrophic zone of Hspg2$^{-/-}$ mice, which is one of the characteristics of the defects in perlecan-deficient cartilage in mice and humans (Arikawa-Hirasawa et al., 1999)(Fig. 6A). In addition, although the calcified matrix was observed only in the last few layers of hypertrophic chondrocytes in wild-type mice, the calcified matrix was found in multiple layers in the hypertrophic zone in perlecan-deficient mice, suggesting impaired remodeling of the calcified cartilage matrix. The expression of OPN mRNA, a marker of terminally differentiated mature chondrocytes, was significantly increased in chondrocytes in Hspg2$^{-/-}$ mice compared with those in wild-type mice (Fig. 6B). In wild-type growth plates, perlecan (red) was expressed and surrounded hypertrophic

Please cite this article as: Ishijima, M., et al., Perlecan modulates VEGF signaling and is essential for vascularization in endochondral bone formation, Matrix Biology (2012), doi:10.1016/j.matbio.2012.02.006

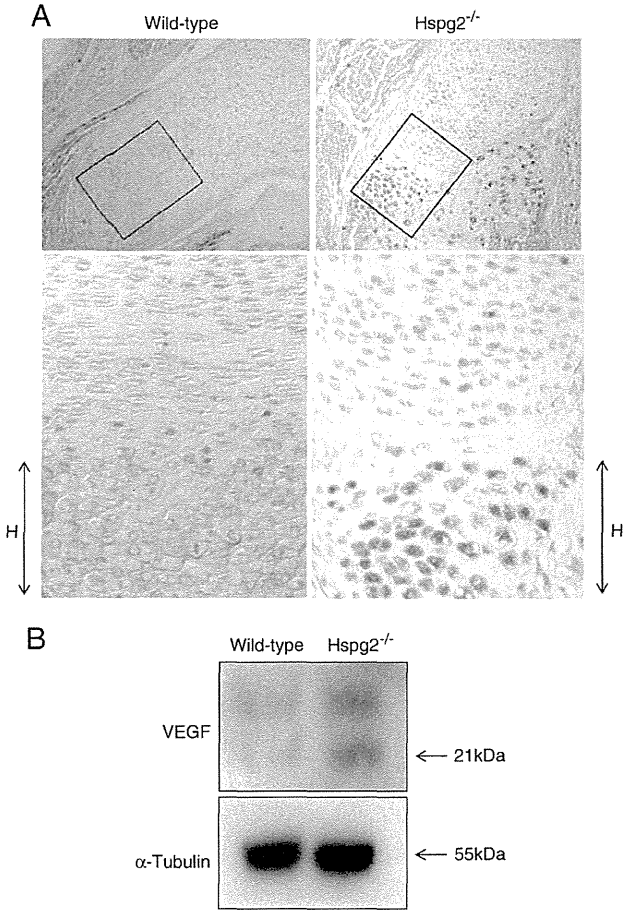

Fig. 3. Increased VEGF expression by chondrocytes in Hspg2$^{-/-}$ mice. (A) Immunostaining of VEGFA. Expression of VEGFA in prehypertrophic and hypertrophic chondrocytes was increased in Hspg2$^{-/-}$ mice compared to that in wild-type mice. Hypertrophic zone (H). (B) Western blot of VEGFA protein. The expression level of the VEGFA proteins was increased further in the chondrocytes of Hspg2$^{-/-}$ mice compared to that in wild-type mice.

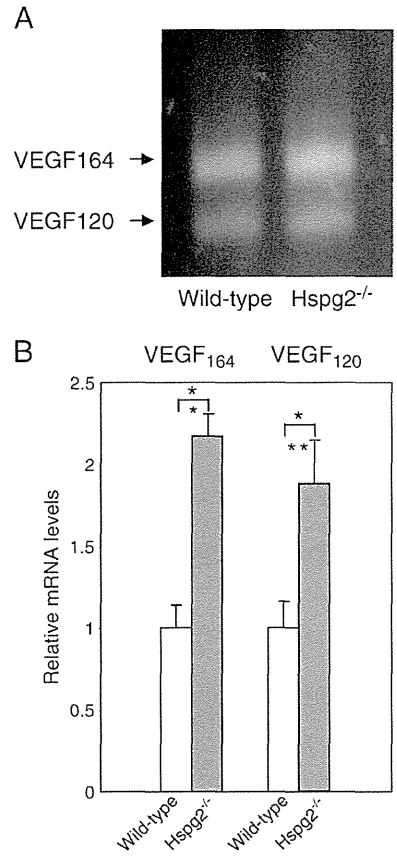

Fig. 4. $VEGF_{164}$ expression is increased in chondrocytes of Hspg2$^{-/-}$ mice. (A) Semi-quantitative RT-PCR of VEGF isoforms. $VEGF_{120}$ and $VEGF_{164}$ mRNA were expressed in chondrocytes prepared from the growth plates of wild-type mice. Expression levels of $VEGF_{164}$ mRNA were most prominent in wild-type mice. In Hspg2$^{-/-}$ mice, these VEGF mRNA were also expressed, with the highest level for $VEGF_{164}$. (B) Real-time RT-PCR analysis of the expression levels of VEGF mRNA in chondrocytes in wild-type and Hspg2$^{-/-}$ mice. $VEGF_{120}$ and $VEGF_{164}$ mRNA were increased in the chondrocytes of Hspg2$^{-/-}$ mice. The increase in the levels of $VEGF_{164}$ mRNA was largest in the absence of perlecan. The relative expression levels of each isoform in wild-type mice were set as 1. *Indicates $p<0.05$.

chondrocytes, while perlecan was absent in Hspg2$^{-/-}$ mice (Fig. 6C) (Xu et al., 2010).

Immunohistochemical analyses revealed that the OPN protein (green) was expressed at the end layer of hypertrophic chondrocytes in wild-type mice. However, in Hspg2$^{-/-}$ growth plates, OPN protein expression was observed in multiple layers of hypertrophic chondrocytes (Fig. 6C). These results suggest that remodeling of the hypertrophic matrix was inhibited in Hspg2$^{-/-}$ mice.

2.7. Inhibition of vascular invasion is due to the defect of perlecan in chondrocytes, but not in endothelial cells

Perlecan is expressed not only in chondrocytes but also in all basement membranes, including vessel walls. Therefore, the inhibition of vascular invasion in the hypertrophic zone in the absence of perlecan could have been due to the absence of perlecan in the basement membranes of endothelial cells. To exclude this possibility, mice in which perlecan was expressed specifically in chondrocytes were created by introducing the transgene (Per-Tg) under the control of a cartilage-specific Col2a1 promoter and enhancer in the Hspg2$^{-/-}$ genetic background (Hspg2$^{-/-}$-Tg mice) (Xu et al., 2010). In the Hspg2$^{-/-}$-Tg mice, perlecan is expressed in cartilage but absent in the basement membranes of blood vessels, muscle, and other tissues surrounding cartilage (Xu et al., 2010). The bone sizes of the HSPG2$^{-/-}$-Tg mice were similar to those of wild-type mice (Fig. 7A). Histological analysis showed that the columnar structure of the growth plate can be restored in Hspg2$^{-/-}$-Tg mice (Fig. 7B). Type II collagen, type X collagen, and osteopontin expression of Hspg2$^{-/-}$-Tg mice were similar to those of wild-type mice.

Vascular invasion into the chondro-osseous region observed in the Hspg2$^{-/-}$-Tg mice was also similar to that of wild-type mice (Fig. 7D). Since Hspg2$^{-/-}$-Tg mice expressed perlecan in cartridge but not surrounding tissues, these results indicate that the inhibition of vascular invasion in Hspg2$^{-/-}$mice is due to the absence of perlecan in cartilage but not to its absence in endothelial cells.

2.8. Perlecan promotes VEGF-induced VEGFR2 activation in endothelial cells

$VEGF_{164}$ is expressed in hypertrophic chondrocytes and is critical for inducing vascular invasion into the hypertrophic zone (Zelzer et al., 2004). As $VEGF_{164}$ contains a heparan sulfate binding site, perlecan may bind to $VEGF_{164}$, which promotes VEGF signaling of endothelial cells for angiogenesis. We tested the binding of purified perlecan from cartilage to $VEGF_{164}$ in a solid phase binding assay

Please cite this article as: Ishijima, M., et al., Perlecan modulates VEGF signaling and is essential for vascularization in endochondral bone formation, Matrix Biology (2012), doi:10.1016/j.matbio.2012.02.006

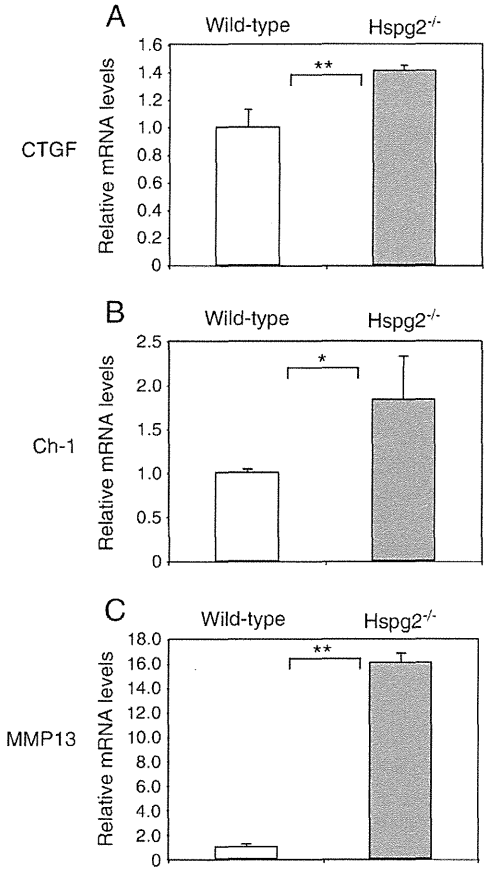

Fig. 5. Expression of molecules involved in vascular invasion. (A, B) Quantitative RT-PCR. Expression of mRNA for the connective tissue growth factor (CTGF) and chondromodulin-1 (Ch-1), which are known to be involved in vascular invasion in endochondral ossification, were significantly increased in chondrocytes from Hspg2$^{-/-}$ mice compared to those in wild-type mice. * and ** indicate $p<0.05$ and <0.01, respectively. **(C)** Expression of MMP13, which is expressed by hypertrophic chondrocytes, was strongly increased in the growth plates of Hspg2$^{-/-}$ mice. **Indicates $p<0.01$.

using perlecan-coated dishes with different amounts of growth factors or growth factor receptors (Fig. 8A). Perlecan bound to FGF2 and to FGF receptors 2 and 3, as reported (Knox et al., 2002; Knox and Whitelock, 2006; Patel et al., 2007; Smith et al., 2007). Perlecan bound to VEGF receptor 2 (VFGFR2), in agreement with recent findings (Goyal et al., 2011). However, perlecan did not bind to $VEGF_{164}$. To test whether perlecan promotes $VEGF_{164}$-mediated VEGFR2 activation, primary endothelial cells from wild-type mouse skin were incubated with $VEGF_{164}$ in the presence of various amounts of perlecan. After being incubated for 5 min at 37 °C, the cells were lysed, and VEGFR2 was immunoprecipitated with anti-VEGFR2 antibody. The proteins were analyzed with Western blotting using anti-pVEGFR2 (Tyr951) and anti-VEGFR2 antibodies as described in the Materials and Methods section. We found that perlecan promoted VEGFR2 phosphorylation (Fig. 8B). The cartilage perlecan-promoted activation of VEGF/VEGFR2 is consistent with the VEGFR2 activation by perlecan from endothelial cells (Zoeller et al., 2009; Goyal et al., 2011).

3. Discussion

Endochondral bone formation occurs through highly coordinated biological processes, including chondrocyte hypertrophy, deposition and remodeling of the cartilage matrix, vascular invasion, apoptosis, osteoblast replacement, and subsequent trabecular bone formation. In this study, we demonstrated that perlecan present in cartilage, but not in capillary basement membranes, is essential for cartilage matrix remodeling, vascular invasion, and the formation of bone marrow and trabecular bone.

Perlecan had been suggested to play crucial roles not only in vasculogenesis but also in the maturation and maintenance of differentiated tissues, including cartilage (Handler et al., 1997). In growth plates of Hspg2$^{-/-}$ mice, the matrix structure is disorganized, and glycosaminoglycans are reduced (Fig. 1A) (Arikawa-Hirasawa et al., 1999; Costell et al., 1999). Biochemical studies in vitro confirmed that perlecan is required for cartilage collagen fibril formation (Kvist et al., 2006). In Hspg2$^{-/-}$ mice, growth plate cartilage is wider, and chondrocytes are located more sparsely in the cartilage matrix than in wild-type mice (Fig. 1). These phenotypes are different from those of cartilage-deficient (cmd/cmd) mice, which are caused by the absence of functional aggrecan, a major chondroitin sulfate proteoglycan in cartilage (Watanabe et al., 1994). These cmd/cmd mice die perinatally; the width of the cartilage of the long bone is narrow, and chondrocytes are rather densely packed in the matrix (Watanabe and Yamada, 2002). In the absence of perlecan, chondrocytes were able to differentiate into mature hypertrophic chondrocytes, which express VEGF (Figs. 3 and 4), MMP13 (Fig. 5C), and osteopontin (Fig. 6B,C). Removal of the hypertrophic matrix and its calcified regions is essential for endochondral bone formation. In wild-type growth plates, only a few layers containing osteopontin and calcification surround mature hypertrophic chondrocytes in the chondro-osseous boundary (Fig. 6). However, in Hspg2$^{-/-}$ growth plates, multiple layers were accumulated near the end of the hypertrophic zone, indicating that hypertrophic cartilage removal was inhibited in the absence of perlecan (Fig. 6). Matrix metalloproteinases, such as MMP-9 and MMP-13, are involved in degradation of the hypertrophic matrix (Vu et al., 1998; Engsig et al., 2000; Inada et al., 2004; Stickens et al., 2004). However, we found that MMP-13 expression was increased in Hspg2$^{-/-}$ growth plates compared to those of wild-type mice. MMP-9 is also expressed in the growth plates of Hspg2$^{-/-}$ mice. Since perlecan interacts with MMPs and is most abundantly expressed in the hypertrophic zone compared with other chondrocyte zones, perlecan may play a role in the activation of MMPs for cartilage remodeling.

Although matrix components are expressed in the cartilage of Hspg2$^{-/-}$ growth plates, the fibrillar formation and density are especially reduced in the hypertrophic zone (Gustafsson et al., 2003). In addition, the columnar structure of hypertrophic chondrocytes is disorganized, and the hypertrophic matrix is often disrupted in Hspg2$^{-/-}$ mice, especially during later stages such as birth (Arikawa-Hirasawa et al., 1999; Costell et al., 1999; Arikawa-Hirasawa et al., 2002). These observations suggest that perlecan provides the strength and rigidity of the hypertrophic matrix structure by interacting with matrix molecules for proper growth plate development. In Hspg2$^{-/-}$ growth plates, the ossified periosteum is formed but apparently curved into the hypertrophic zone, in contrast to the longitudinal growth seen in bone collars of wild-type mice (Fig. 1). Because the formation of bone marrow and the trabecular bone was severely inhibited, the bone collar structure separated two adjacent cartilage molds within the humerus close together (Fig. 1). The abnormal alignment of the bone collar seen in Hspg2$^{-/-}$ growth plates is likely due in part to the less rigid hypertrophic matrix structure.

In addition to MMP-9 and MMP-13, other molecules, such as CTGF (CCN2) and Ch-1, are implicated in matrix remodeling and vascular invasion in the growth plates (Ivkovic et al., 2003). In Hspg2$^{-/-}$ growth plates, the expression levels of CTGF and Ch-1 were significantly increased (Fig. 5). VEGFA plays an important role in angiogenesis for endochondral ossification. Administration of an inhibitor of VEGFA activity in mice reduced vascular invasion into the hypertrophic zone and inhibited endochondral bone formation (Gerber et al.,

Please cite this article as: Ishijima, M., et al., Perlecan modulates VEGF signaling and is essential for vascularization in endochondral bone formation, Matrix Biology (2012), doi:10.1016/j.matbio.2012.02.006

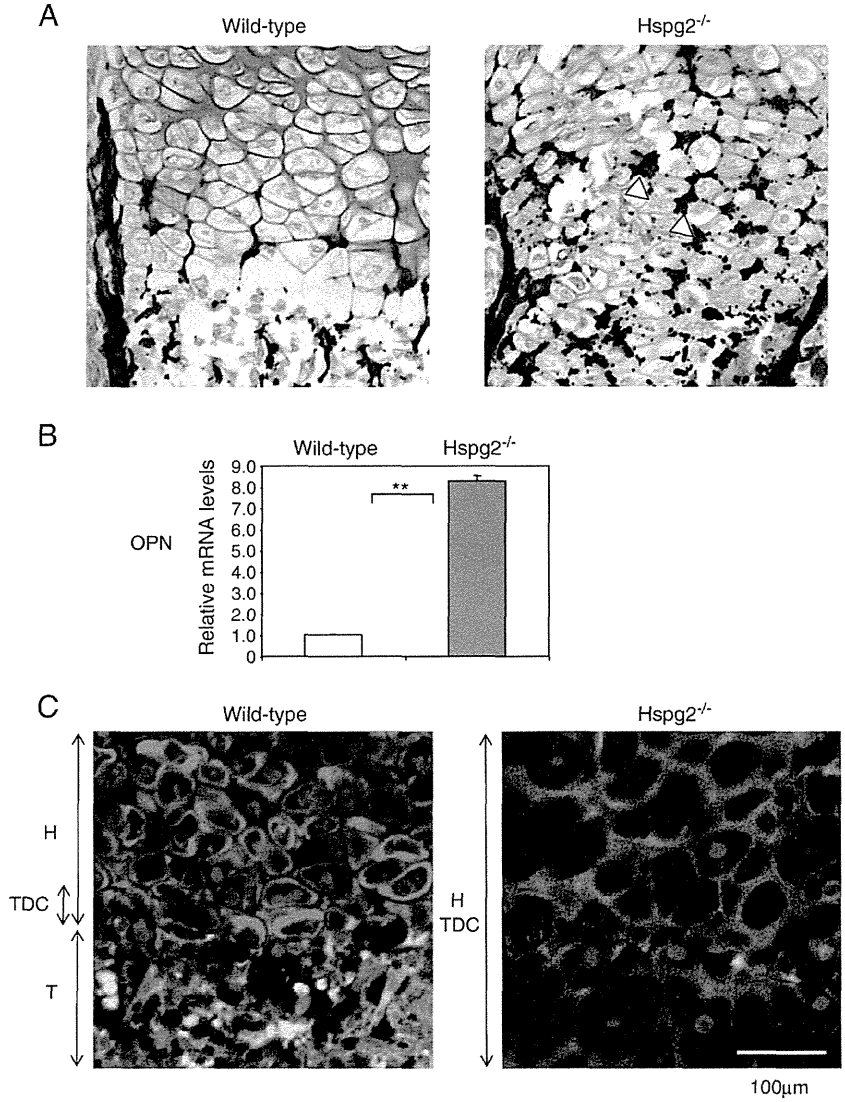

Fig. 6. Accumulation of mature population of hypertrophic chondrocytes in the growth plates of Hspg2$^{-/-}$ mice. **(A)** Double staining of Safranin-O (red) and von Kossa (brown) staining at the proximal end of the humerus in E18.5 wild-type and Hspg2$^{-/-}$ mice. In E18.5 Hspg2$^{-/-}$ mice, the matrix surrounding multiple layers of hypertrophic chondrocytes is calcified, whereas in the wild-type growth plate, the matrix surrounding only a few hypertrophic layers at the end of cartilage is calcified. Arrowheads indicate the formation of hydroxyapatite nodules (calcospherites) in the hypertrophic zone of Hspg2$^{-/-}$ mice. (B) Real-time RT-PCR analysis. Osteopontin OPN mRNA expression was significantly increased in the chondrocytes of E18.5 Hspg2$^{-/-}$ mice compared with the expression in wild-type mice. ** indicates $p<0.01$. **(C)** Double immunostaining for OPN (green) and perlecan (red) of the proximal end of the humerus in E18.5 wild-type and Hspg2$^{-/-}$ mice. OPN-expressing mature hypertrophic chondrocytes accumulated in the growth plates of Hspg2$^{-/-}$ mice. Only a few hypertrophic cell layers expressed OPN in the terminally differentiated chondrocyte area (TDC) of the wild-type mice . Perlecan was expressed in the area of hypertrophic chondrocytes (H) and TDC, but not in the trabecular bone area (T) of the growth plate of wild-type mice. Perlecan was completely absent in all of these areas in Hspg2$^{-/-}$ mice. Scales show 100 μm in length. (For interpretation of the references to color in this figure legend, the reader is referred to the web version of this article.)

1999). Conditional VEGFA knockout in mice specific in chondrocytes using Col2a1Cre displayed an expansion of the hypertrophic zone, delayed vascular invasion, and impaired endochondral ossification (Zelzer et al., 2004). Forced expression of Runx2 in hypertrophic chondrocytes using the Col10a1 promoter reduced VEGFA expression and resulted in impaired cartilage matrix remodeling and an almost complete lack of bone marrow due to the inhibition of vascular invasion into hypertrophic cartilage (Hattori et al., 2010). In the Hspg2$^{-/-}$ growth plates, the VEGF protein levels were increased. $VEGF_{120}$ and $VEGF_{164}$ mRNA were expressed in the growth plates of wild-type mice. The mRNA expression levels for $VEGF_{120}$ and $VEGF_{164}$ were increased in Hspg2$^{-/-}$ growth plates, with the highest level for $VEGF_{164}$ (Fig. 4B). In the zebrafish, perlecan regulates angiogenic blood vessel formation, and perlecan knockdown results in an abnormal increase and relocation of the VEGFA proteins (Zoeller et al., 2009). In wild-type mice, perlecan is expressed not only in cartilage but also in blood vessel basement membranes. We therefore examined whether cartilage or endothelial perlecan is important for normal vascular invasion into the hypertrophic zone and endochondral bone formation by expressing the perlecan (Hspg2) transgene (Tg) specifically in the cartilage of HSPG2$^{-/-}$ mice (Xu et al., 2010). The mutant mice (Hspg2$^{-/-}$-Tg) expressed perlecan in cartilage but not in surrounding tissues (Fig. 7C)(Xu et al., 2010). Hspg2$^{-/-}$-Tg mice survived and showed normal cartilage development and endochondral bone formation (Fig. 7A, B, D). These results suggest that perlecan is critical in cartilage but not in endothelial cell basement membranes for vascular invasion into the hypertrophic zone. Since vascularization in other tissues

Please cite this article as: Ishijima, M., et al., Perlecan modulates VEGF signaling and is essential for vascularization in endochondral bone formation, Matrix Biology (2012), doi:10.1016/j.matbio.2012.02.006

occurred without perlecan, the mechanism of angiogenesis must be unique in endochondral ossification processes.

Perlecan purified from bovine cartilage enhanced the activation of $VEGF_{164}$-VEGFR2 signaling in endothelial cells (Fig. 8). This activation is facilitated via direct binding of perlecan to VEGFR2 (Fig. 8A). Perlecan from endothelial cell culture and recombinant endorepellin, the C-terminal part of perlecan, binds to VEGFR1 and 2 (Goyal et al., 2011). Perlecan promotes angiogenesis, while its fragment acts as an anti-angiogenic factor by disrupting the actin assembly of endothelial cells through interaction with α2β1 integrin (Bix et al., 2004). Endorepellin attenuated VEGFA-mediated activation of VEGFR2 in endothelial cells, and this attenuation is required for α2β1 integrin (Goyal et al., 2011). Cartilage perlecan did not bind to $VEGF_{164}$, while endothelial cell perlecan binds to the heparin-binding site containing VEGFA (Goyal et al., 2011). This difference may be because cartilage perlecan is substituted with not only heparan sulfate chains but also chondroitin sulfate chains, which may inhibit perlecan interactions with $VEGF_{164}$.

Studies by Takimoto et al., (Takimoto et al., 2009), with overexpression of VEGFA in cartilage in transgenic mice and in chick embryonic forelimbs, revealed the perichondrium prevents vascular invasion into cartilage from highly vascularized surrounding tissues at early stages, but at later stages, perichondrial angiogenesis occurs and is followed by vascular invasion into the hypertrophic zone. This process is required for heparin-binding VEGF isoforms. In $Hspg2^{-/-}$ mice, heparin-binding $VEGF_{164}$ was excessively expressed in the hypertrophic zone, and vasculature in the perichondrium and bony collar was observed, but osteoclasts were reduced, and vascular invasion was inhibited (Fig. 2A). Since perlecan is not expressed in the perichondrium (data not shown) (Melrose et al., 2004; Smith et al., 2010), other molecules, such as Nrp1 and Nrp2, which are expressed in the vasculature of surrounding tissues (Takimoto et al., 2009), enhance VEGFR2 signaling via binding to VEGFA as a receptor (Staton et al., 2007; Herve et al., 2008).

In summary, we demonstrated that perlecan in cartilage is essential for vascular invasion from the perichondrium into the hypertrophic zone. We showed that cartilage perlecan enhances VEGF/

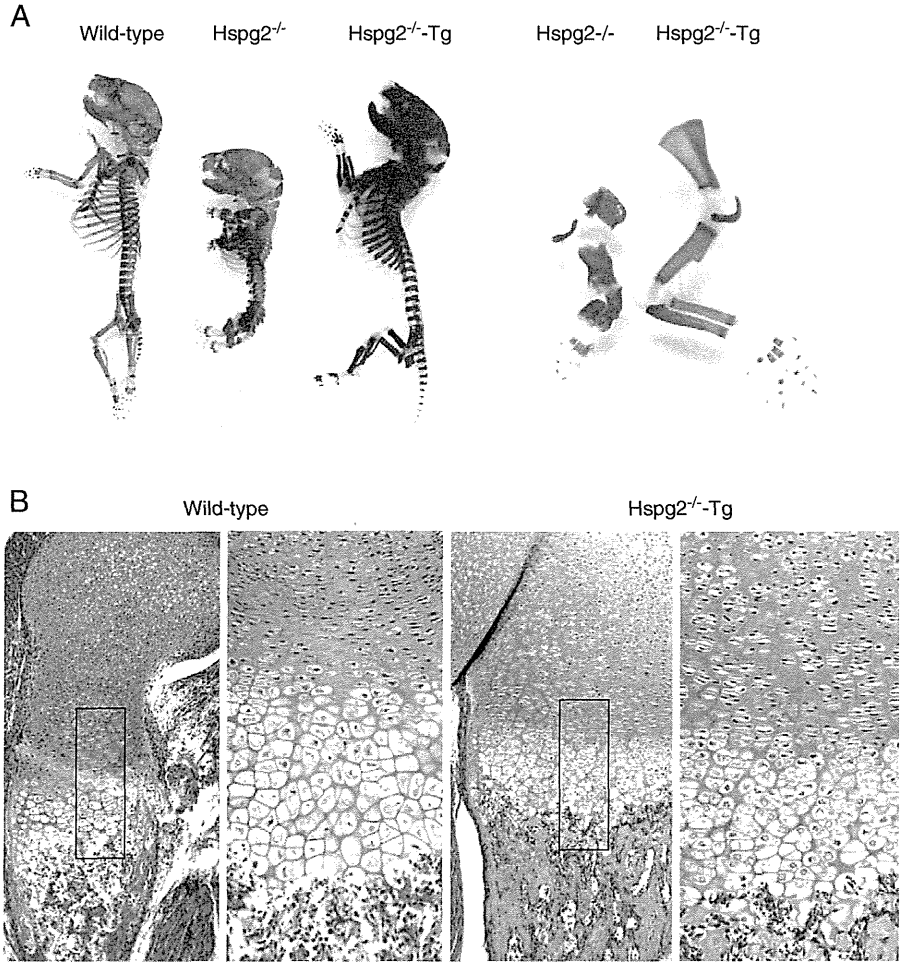

Fig. 7. Restore skeletal abnormalities of $Hspg2^{-/-}$ mice to normal by mating with transgenic mice (Col2a1-PerTg). (A) Skeletal abnormalities of $Hspg2^{-/-}$ mice were rescued by creating $Hspg2^{-/-}$-Tg mice containing the Hspg2 transgene (Col2a1-PerTg) under the control of a chondrocyte-specific Col2a1 promoter and enhancer. The left three panels show skeletal preparations of E18.5 whole embryos (wild-type, $Hspg2^{-/-}$, and $Hspg2^{-/-}$-Tg); the right two panels show hind limbs from E18.5 $Hspg2^{-/-}$ and $Hspg2^{-/-}$-Tg mice. Cartilage was stained with Alcian blue, and bone was stained with Alizarin red S. (B) Histological sections of the growth plate of E18.5 hind limbs of wild-type mice stained with H-E. Columnar structure of the growth plate was restored in $Hspg2^{-/-}$-Tg mice. (C) Immunostaining of extracellular matrix proteins in E18.5 growth plates from wild-type and $Hspg2^{-/-}$-Tg mice. Perlecan was expressed in the growth plates of $Hspg2^{-/-}$-Tg mice. Expression of type II collagen (Col2), type X collagen (Col10), and osteopontin (OPN) was similar for the wild-type and $Hspg2^{-/-}$-Tg mice. **(D)** Immunostaining of CD31 in the growth plate of E18.5 wild-type and $Hspg2^{-/-}$-Tg mice. The vascular invasion of the chondro-osseous boundary and bone marrow observed in $Hspg2^{-/-}$-Tg mice was similar to that in wild-type mice.

Please cite this article as: Ishijima, M., et al., Perlecan modulates VEGF signaling and is essential for vascularization in endochondral bone formation, Matrix Biology (2012), doi:10.1016/j.matbio.2012.02.006

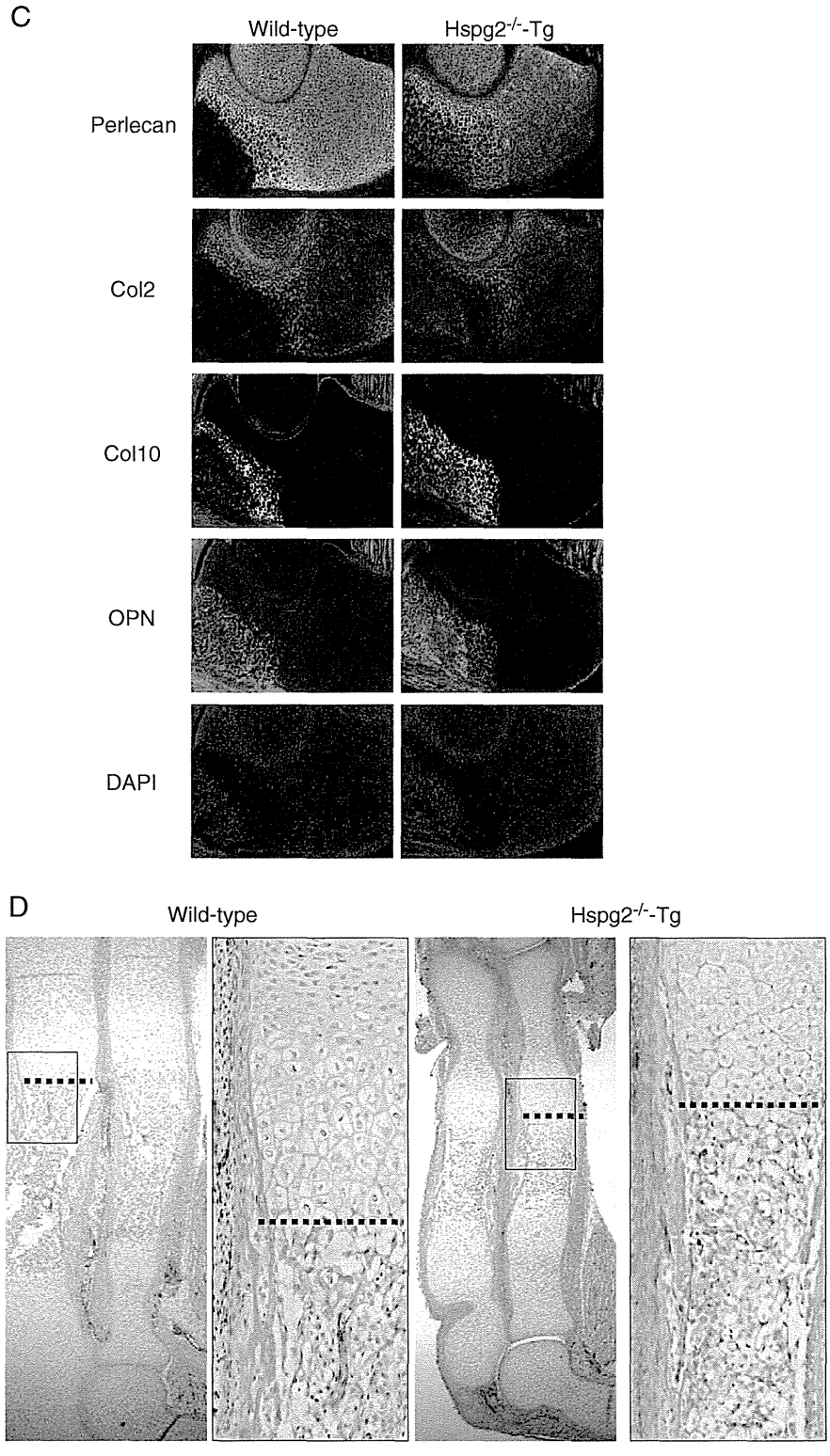

Fig. 7 (*continued*)

VEGFR signaling of endothelial cells in culture. In Hspg2$^{-/-}$ growth plates, hypertrophic chondrocytes express molecules such as MMP-13, OPN, CTGF, and VEGFA, which are important for cartilage matrix remodeling and for vascular invasion. However, without perlecan in cartilage, the osteopontin-expressing hypertrophic chondrocyte layers and calcified areas expand, and formation of bone marrow and the trabecular bone is inhibited. The defect in vascular invasion results in the inhibition of cartilage remodeling and replacement of

Please cite this article as: Ishijima, M., et al., Perlecan modulates VEGF signaling and is essential for vascularization in endochondral bone formation, Matrix Biology (2012), doi:10.1016/j.matbio.2012.02.006

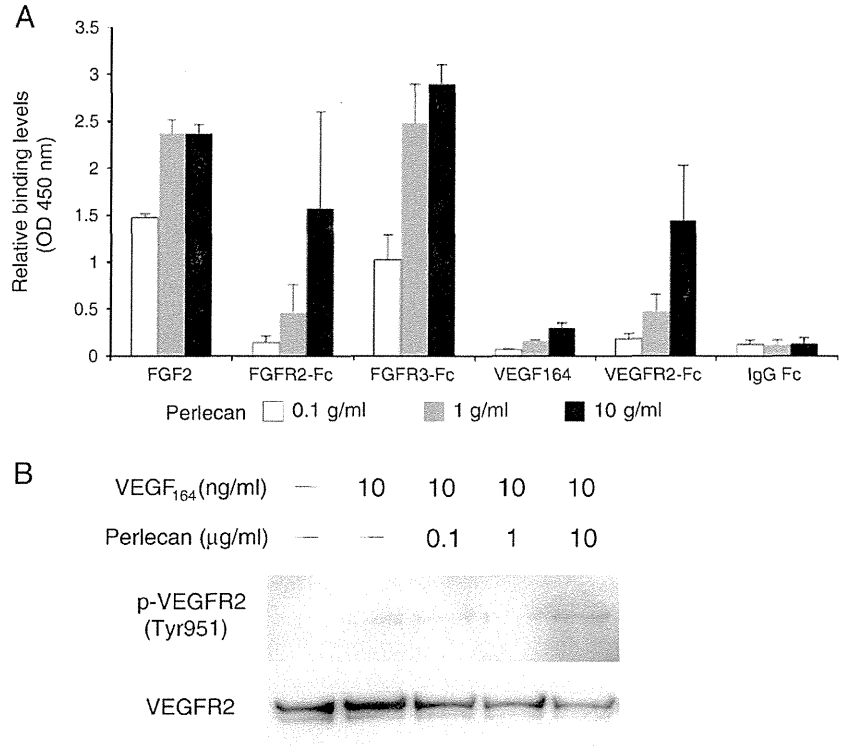

Fig. 8. Perlecan binds to VEGFR2 and promotes VEGF-induced VEGFR2 activation in endothelial cells. Binding of cartilage perlecan to FGF2 and $VEGF_{164}$ and their receptors at various concentrations in solid phase assays. Perlecan bound to FGF2 and FGFR2. Perlecan did not bind to $VEGF_{164}$ but bound to its receptor, VEGFR2. (B) Western blots of VEGFR2 and phosphorylated VEGFR2 of endothelial cells treated with $VEGF_{164}$ and perlecan. Perlecan promoted the phosphorylation levels of VEGFR2 in the presence of VEGFA.

hypertrophic chondrocytes with osteoblasts, which leads to severe defects in endochondral bone formation of $Hspg2^{-/-}$ mice.

4. Experimental procedures

4.1. Mice

Perlecan knockout ($Hspg2^{-/-}$) mice were generated as described previously (Arikawa-Hirasawa et al., 1999). About half of the $Hspg2^{-/-}$ mice died around embryonic day (E) 10 of hemorrhage due to defective myocardium basement membranes (Arikawa-Hirasawa et al., 1999; Costell et al., 1999; Xu et al., 2010). Perinatal lethality-rescued perlecan knockout mice ($Hspg2^{-/-}$-Tg, $Hspg2^{-/-}$; Col2a1-$Hspg2^{Tg/-}$) were created by expressing a transgene for perlecan under the control of the Col2a1 promoter and enhancer specifically to cartilage (Col2a1-PerTg) in $Hspg2^{-/-}$ mice (Xu et al., 2010). The animal protocol approved by the NIDCR ACU Committee was used for maintaining and handling mice, and all mice were housed in a mouse facility affiliated with the American Association for the Accreditation of Laboratory Animal Care.

4.2. Skeletal histology

Paraffin sections (5 μm) of mouse embryos were deparaffinized using xylene, rehydrated through an alcohol gradient series to water, and then used for histological and immunohistochemical analysis. Paraformaldehyde (4%) was used for fixation in histology and immunohistochemistry. Double staining for Safranin-O and von Kossa staining was performed as described (Aszodi et al., 2003). Immunostaining was performed using a Histostain-SP kit (Zymed) according to the manufacturer's instructions. The following antibodies were used for immunohistochemical studies: a rabbit polyclonal antibody for perlecan from Dr. T. Sasaki (University of Erlangen-Nuremberg, Erlangen, Germany), a monoclonal antibody for osteopontin (R&D Systems), a monoclonal antibody for VEGF (R&D Systems), a monoclonal antibody for type II collagen (Hybridoma Bank, University of Iowa), and a type X collagen chain from Greg Lunstrum (Shriners Hospital for Children Research Center, Portland). Immunostaining for CD31 was performed using a monoclonal antibody for CD31 (Pharmingen) as described previously (Colnot et al., 2005). For the immunofluorescence study, fluorescein isothiocyanate (FITC)-conjugated or Alexa-488-conjugated (Jackson ImmunoResearch Laboratories) was used as a secondary antibody. Tartrate-resistant acid phosphatase (TRAP) was stained as described previously (Ishijima et al., 2001, 2007).

4.3. Skeletal analysis

Bones and cartilage of newborn mice were stained with Alizarin red and Alcian blue as described previously (Arikawa-Hirasawa et al., 1999). The bone length and width were histologically measured, and the relative length and width of the humeri in the wild-type mice were set at 100%.

4.4. RT-PCR analysis

Total RNA was extracted from growth plate cartilage of the distal end of the femora and the proximal end of the tibiae of E16.5 or E18.5 embryos using TRIzol (Invitrogen).

For reverse transcription, 2 μg of total RNA were used to generate cDNA, which was used as a template for PCRs with gene-specific primers. cDNA was amplified with an initial denaturation at 95 °C for 3 min, and then at 95 °C for 30 s, 60 °C for 30 s, and 72 °C for 30 s for 25 cycles. A final elongation step was conducted at 72 °C for 5 min, and then the cDNA was separated on agarose gels. Real-time PCR analysis was performed using a TaqMan Real-Time PCR detection system (ABI7000,

Please cite this article as: Ishijima, M., et al., Perlecan modulates VEGF signaling and is essential for vascularization in endochondral bone formation, Matrix Biology (2012), doi:10.1016/j.matbio.2012.02.006

Applied Biosystems). TaqMan Universal Master Mix and TaqMan Gene Expression Assays Hs99999901_s1 and Hs01078483_g1 (Applied Biosystems) were used according to the manufacturer's protocol, with a final reaction volume of 25 µl. Sequences for VEGF-120, -164, -188, CTGF, Ch-1, MMP13, and OPN specific PCR primers are available from the authors upon request.

4.5. Western blotting

Growth plate cartilage of the distal end of the femora and the proximal end of the tibiae of E16 mice was dissected from the right side of the knee joint and then lysed. The lysates were run on a 10% SDS-PAGE. A monoclonal antibody for VEGF (C-1, Santa Cruz) was used for Western blot analysis.

For the phosphorylation assay of VEGFR2, primary endothelial cells were prepared from the wild-type mouse skin at postnatal day 4 by immunopanning using anti-ICAM2 antibody (BD Biosciences), as described previously (Kataoka et al., 2003). The endothelial cells were cultured in DMEM: F12 = 1:1 (Invitrogen) containing 100 µM nonessential amino acid (Invitrogen), 20% fetal calf serum (FCS; Hyclone), 100 µg/ml heparin (Sigma-Aldrich), 100 U penicillin (Invitrogen), 100 µg/ml streptomycin (Invitrogen), and 50 µg/ml endothelial cell growth supplement (ECGS; BD Biosciences). For starvation of the phosphorylation assay, FCS, heparin, and ECGS were eliminated from the medium, and endothelial cells were incubated overnight. $VEGF_{164}$ and various amounts of perlecan were mixed and preincubated at room temperature for 1 h. After preincubation, the mixture of $VEGF_{164}$ and perlecan was added to the starved endothelial cell culture, and the cells were incubated for 5 min at 37 °C. The cells were lysed with the lysis buffer (1% Triton-X100, 1.5 mM EDTA, 1 mM Na_3PO_4, 25 mM NaF, and 1 mM Na_3VO_4 in Tris-buffered saline) for 5 min on ice. The cell lysate was centrifuged at 15,000 rpm for 30 min at 4 °C and separated from the cell pellet. Fifty µg of the cell lysate was incubated with anti-VEGFR2 antibody (Cell Signaling) in the binding/washing buffer (0.1% Triton-X100, 1.5 mM EDTA, 1 mM Na_3PO_4, 25 mM NaF, and 1 mM Na_3VO_4 in Tris-buffered saline) for 1 h at 4 °C. Then, protein-G Sepharose beads (Invitrogen) were added to the reaction mixture and incubated for 1 h at 4 °C. After incubation, the beads were washed with the binding/washing buffer. Proteins bound to the beads were eluted with the LDS-sample buffer (Invitrogen) with 10 µM DTT. The proteins were detected with Western blotting using anti-pVEGFR2 (Tyr951) and anti-VEGFR2 antibodies (Cell Signaling).

4.6. Binding assays

A solid phase binding assay was performed using purified perlecan from bovine cartilage (Govindraj et al., 2002). Two hundred and fifty ng of perlecan was coated onto 96-well plates at 4 °C overnight. The wells were blocked with the blocking buffer (3% bovine serum albumin: Sigma-Aldrich) at room temperature for 2 h. After blocking, various amounts of FGF-basic (PeproTech), $VEGF_{164}$ (R&D Systems), and recombinant fusion proteins of extracellular domains of FGFR2, FGFR3, and VEGFR2 with the human IgG Fc portion (R&D Systems) in the blocking buffer were added and incubated at room temperature for 1 h. The proteins bound to perlecan were detected with anti-FGF-basic (Millipore), anti-VEGF (Santa Cruz Biotech.), biotinylated anti-human IgG (Jackson ImmunoResearch Inc.), and horseradish peroxidase (HRP)-conjugated secondary antibodies (Thermo) and streptavidin (Sigma-Aldrich). After incubation with appropriate antibodies, 3,3',5,5'-tetramethyl-benzidine solution (Sigma-Aldrich) was added to the wells and incubated for 10 min at room temperature. After 0.5 N H_2SO_4 was added to stop the colorimetric reaction by HRP, the optical density at 450 nm was measured using a microplate reader (Safire, Tecan Ltd.).

4.7. Statistical analysis

Group means were compared with analysis of variance, and the significance of differences was determined by using an unpaired *t*-test. *P* values less than 0.05 were considered significant.

Acknowledgments

This work was supported by the Intramural Program of the NIDCR, NIH (Y.Y.), and grant-in-aid (to 19791047 and 21791418 for M.I and 22300223 for E.A-E) from the Ministry of Education, Science, and Culture of Japan. M.I., N.S., K.H., and T.M. were supported in part by a fellowship from the Japan Society for the Promotion of Science.

References

Arikawa-Hirasawa, E., Watanabe, H., Takami, H., Hassell, J.R., Yamada, Y., 1999. Perlecan is essential for cartilage and cephalic development. Nat Genet 23, 354–358.

Arikawa-Hirasawa, E., Wilcox, W.R., Le, A.H., Silverman, N., Govindraj, P., Hassell, J.R., Yamada, Y., 2001a. Dyssegmental dysplasia, Silverman–Handmaker type, is caused by functional null mutations of the perlecan gene. Nat Genet 27, 431–434.

Arikawa-Hirasawa, E., Wilcox, W.R., Yamada, Y., 2001b. Dyssegmental dysplasia, Silverman–Handmaker type: unexpected role of perlecan in cartilage development. Am J Med Genet 106, 254–257.

Arikawa-Hirasawa, E., Le, A.H., Nishino, I., Nonaka, I., Ho, N.C., Francomano, C.A., Govindraj, P., Hassell, J.R., Devaney, J.M., Spranger, J., Stevenson, R.E., Iannaccone, S., Dalakas, M.C., Yamada, Y., 2002. Structural and functional mutations of the perlecan gene cause Schwartz–Jampel syndrome, with myotonic myopathy and chondrodysplasia. Am J Hum Genet 70, 1368–1375.

Aszodi, A., Hunziker, E.B., Brakebusch, C., Fassler, R., 2003. Beta1 integrins regulate chondrocyte rotation, G1 progression, and cytokinesis. Genes Dev 17, 2465–2479.

Aviezer, D., Hecht, D., Safran, M., Eisinger, M., David, G., Yayon, A., 1994. Perlecan, basal lamina proteoglycan, promotes basic fibroblast growth factor-receptor binding, mitogenesis, and angiogenesis. Cell 79, 1005–1013.

Bix, G., Fu, J., Gonzalez, E.M., Macro, L., Barker, A., Campbell, S., Zutter, M.M., Santoro, S.A., Kim, J.K., Hook, M., Reed, C.C., Iozzo, R.V., 2004. Endorepellin causes endothelial cell disassembly of actin cytoskeleton and focal adhesions through alpha2beta1 integrin. J Cell Biol 166, 97–109.

Brandau, O., Aszodi, A., Hunziker, E.B., Neame, P.J., Vestweber, D., Fassler, R., 2002. Chondromodulin I is dispensable during enchondral ossification and eye development. Mol Cell Biol 22, 6627–6635.

Brown, J.C., Sasaki, T., Gohring, W., Yamada, Y., Timpl, R., 1997. The C-terminal domain V of perlecan promotes beta1 integrin-mediated cell adhesion, binds heparin, nidogen and fibulin-2 and can be modified by glycosaminoglycans. Eur J Biochem 250, 39–46.

Colnot, C., de la Fuente, L., Huang, S., Hu, D., Lu, C., St-Jacques, B., Helms, J.A., 2005. Indian hedgehog synchronizes skeletal angiogenesis and perichondrial maturation with cartilage development. Development (Cambridge, England) 132, 1057–1067.

Costell, M., Gustafsson, E., Aszodi, A., Morgelin, M., Bloch, W., Hunziker, E., Addicks, K., Timpl, R., Fassler, R., 1999. Perlecan maintains the integrity of cartilage and some basement membranes. J Cell Biol 147, 1109–1122.

DeCarlo, A.A., Whitelock, J.M., 2006. The role of heparan sulfate and perlecan in bone-regenerative procedures. J Dent Res 85, 122–132.

Engsig, M.T., Chen, Q.J., Vu, T.H., Pedersen, A.C., Therkidsen, B., Lund, L.R., Henriksen, K., Lenhard, T., Foged, N.T., Werb, Z., Delaisse, J.M., 2000. Matrix metalloproteinase 9 and vascular endothelial growth factor are essential for osteoclast recruitment into developing long bones. J Cell Biol 151, 879–889.

Gerber, H.P., Vu, T.H., Ryan, A.M., Kowalski, J., Werb, Z., Ferrara, N., 1999. VEGF couples hypertrophic cartilage remodeling, ossification and angiogenesis during endochondral bone formation. Nat Med 5, 623–628.

Ghiselli, G., Eichstetter, I., Iozzo, R.V., 2001. A role for the perlecan protein core in the activation of the keratinocyte growth factor receptor. Biochem J 359, 153–163.

Govindraj, P., West, L., Koob, T.J., Neame, P., Doege, K., Hassell, J.R., 2002. Isolation and identification of the major heparan sulfate proteoglycans in the developing bovine rib growth plate. J Biol Chem 277, 19461–19469.

Govindraj, P., West, L., Smith, S., Hassell, J.R., 2006. Modulation of FGF-2 binding to chondrocytes from the developing growth plate by perlecan. Matrix Biol 25, 232–239.

Goyal, A., Pal, N., Concannon, M., Paul, M., Doran, M., Poluzzi, C., Sekiguchi, K., Whitelock, J.M., Neill, T., Iozzo, R.V., 2011. Endorepellin, the angiostatic module of perlecan, interacts with both the alpha2beta1 integrin and vascular endothelial growth factor receptor 2 (VEGFR2): a dual receptor antagonism. J Biol Chem 286, 25947–25962.

Gustafsson, E., Aszodi, A., Ortega, N., Hunziker, E.B., Denker, H.W., Werb, Z., Fassler, R., 2003. Role of collagen type II and perlecan in skeletal development. Ann N Y Acad Sci 995, 140–150.

Handler, M., Yurchenco, P.D., Iozzo, R.V., 1997. Developmental expression of perlecan during murine embryogenesis. Dev Dyn 210, 130–145.

Hattori, T., Muller, C., Gebhard, S., Bauer, E., Pausch, F., Schlund, B., Bosl, M.R., Hess, A., Surmann-Schmitt, C., von der Mark, H., de Crombrugghe, B., von der Mark, K., 2010. SOX9 is a major negative regulator of cartilage vascularization, bone marrow